Design and Control of a6-degree-of-freedom Precision Positioning System

Kunhai Cai[1], Yanling Tian[1*, 2],Fujun Wang[1],Dawei Zhang[1], Xianping Liu[2], Bijan Shirinzadeh[3]

[1]Key Laboratory of Mechanism Theory and Equipment Design of Ministry of Education, Tianjin University, Tianjin 300072, China

[2]School of Engineering, University of Warwick, Coventry CV4 7DL, UK

[3]Robotics and Mechantronics Research Laboratory, Department of Mechanical and Aerospace Engineering, Monash University, VIC 3800, Australia

Abstract: This paper presents the design and test of a6-degree-of-freedom (DOF) precision positioning system, which is assembledby two different 3-DOF precision positioning stages each driven by three piezoelectric actuators (PEAs). Based on the precision PEAs and flexure hinge mechanisms, high precision motion is obtained.The design methodology and kinematic characteristics of the6-DOF positioning system areinvestigated. According to an effective kinematic model, the transformation matrices are obtained, which is used to predict the relationship between the output displacement from the system arrangement and the amountof PEAsexpansion. In addition, the static and dynamic characteristics of the 6-DOF system have been evaluated by finite element method (FEM) simulation andexperiments. The design structure provides a high dynamic bandwidth withthe first naturalfrequency of 586.3 Hz.Decoupling control is proposed to solve the existing coupling motion of the 6-DOF system. Meanwhile, in order to compensate for the hysteresis of PEAs, the inverse Bouc-Wen model was applied as a feedforward hysteresis compensator in the feedforward/feedback hybrid control method. Finally, extensive experiments were

performed to verify the tracking performance of the developed mechanism.

Keywords: 6-DOF positioning system, Piezoelectric actuators (PEAs), Kinematic model, Tracking control.

Nomenclature

a, b,c parameters of Bouc-Wen model

h hysteresis variable

d_{33} piezoelectric constant

Vapplied voltage

$d$displacement output of the free PEA

k_{pzt}stiffness of PEA

$k_c$equivalent stiffness of Hertzian contact

k_{fh}equivalent stiffness in vertical direction of elliptical flexure hinge

X, Y, Z,O Cartesian coordinates of a point

r, R radius of the moving platform and the moving circular ring, respectively

x, y, zdisplacements in the X-, Y-, Z-axes

θ_x, θ_y, αangle rotation about the X, Y-axes and Z-axes

$\boldsymbol{T}^1_{in}$, $\boldsymbol{T}^1_{out}$transformation matrix of the in-plane and out-of-plane 3-DOF stage, respectively.

$\boldsymbol{T}^1$ transformation matrix of the 6-DOF stage

$\boldsymbol{I}$input displacements matrix

$\boldsymbol{O}$output displacements matrix $\boldsymbol{O}$

δ_1, δ_2,$\delta_3$elongation of the PEAs in the in-plane 3-DOFstage

δ_4, δ_5, δ_6 elongation of the PEAs in the out-of-plane3-DOFstage

$P_z$moving coordinate O_d-$X_dY_dZ_d$ relative to thereference coordinate O-XYZ translated along the Z-axis

P_x,P_x and $T_z$moving coordinate O_s-$X_sY_sZ_s$ relative to the coordinate O_d-$X_dY_dZ_d$ translated along the X-, Y- and Z-axis, respectively

$\boldsymbol{T}_d$transformation matrix of the moving coordinate O_d-$X_dY_dZ_d$ relative to the reference coordinate O-XYZ

$\boldsymbol{T}_s$transformation matrix of the moving coordinate O_s-$X_sY_sZ_s$ relative to the reference coordinate O-XYZ

$\boldsymbol{T}_{sd}$transformation matrix of the moving coordinate O_s-$X_sY_sZ_s$ relative to the coordinate O_d-$X_dY_dZ_d$

1. Introduction

Over the past several decades, as one of the best solutions for the micro/nano operating problems in industry, such as nano-imprint, cell operation, scanning probe microscopes, high density data recording, optical instruments, measurement systems and micro/nano manipulations [1-7], a precision positioning system usually possesses a number of advantages such as high positioning accuracy, fast response speed, appropriate workspace, satisfactory stability and dynamic characteristics[8,9].It is mainly composed of three parts,namely, the actuation unit, guide mechanism and end-effector. The piezoelectric actuator (PEA) is the main type of actuator which is often used to drivea positioning mechanismbecause it offers the extremely fine resolution, quick response, large force generation, high electrical-mechanical power conversion efficiency and small volume. Moreover, in order to guarantee positioning accuracy, one of the best choices is to utilize flexure based mechanism for the motion guidance because the flexure based mechanism is capable of improving the motion accuracy due to the advantages of flexure hinges including no backlash, free of wear, no lubrication, and low friction. Thus,it is important to determine the static and dynamic performance of the positioning system.

Recent research efforts have been directed towards the design and control methodologies of multi-DOFs precision positioning systems. The micro/nano operating industry fields are distinguished with respect to systems for planar positioning, systems for out-of-plane positioning and combinations of both.A flexure-based mechanism for ultra-precision operation with 1-DOF, and a 3-DOF planar micro/nano manipulation were presented by Tian et al. [10,11]. Qin et al. focused on design two different type 2-DOF decoupling positioning stages [12,13]. Li et al. proposed a parallel-kinematic high-bandwidth XY nanopositioningstage [14].Cai et al. [15].focused on designa planar 3-DOF stage with T-shape flexible hinge mechanism. In addition, there have also been some out-of-plane positioning systems. A 3-DOF micro-positioning table was investigated in Ref. [16]. Another nanoprecision 3-DOF vertical positioning system was presented in [17], which can be used in various optical alignment systems. Lee et al[18] proposed a three-axis out-of-planenanopositioning stage with a new flexure structure, which had the aperture to measure thebio-specimen. Shao et al[19] presented a novel precision tilt positioning mechanism for inter-satellite optical communication.Furthermore, combinations of in-plane and out-of-plane system have been explored and utilized. A flexure hinge-based XYZ atomic force microscopy scanner was presented by Kim et al[20]. In Ref. [21] a three translational DOF complaint perpendicular parallel micro-manipulator with monolithic structure was proposed. Eichmann et al. [22] designed a high-precision xyz-measuring table for the determination of the 3D dose rate distributions of brachytherapy sources.

From the above literature review, it can be seen that most of the existing precision positioning systems are featured by oneto three-DOF motions[10-22], which cannot meet the needs of manipulations in some cases. For example, an atomic force microscope designed for nanometrology in Ref. [23],which used a 6-DOF nanopositioning stage to carry the sample carrier. Thus, it is necessary to develop novel positioning stages with 6-DOF motions in some special systems, which could extend workspace and improve flexibility of the operation ends.

This paper focuses on the design of a 6-DOF precision positioning system which can be utilizedfor micro/nano operating of the high precision system. Recently, many kinds of 6-DOF precision positioning systems have been reported. A piezoelectric actuator-based micromanipulator with six degrees of freedom was proposed in [24]. Richard et al [25] presented a 6-DOF piezoelectrically actuated fine motion stage that could be used for three-dimensional error compensation with a long-range translation mechanism. Liang et al[26] presented a 6-DOF parallel mechanism based on three inextensible limbs, whichwere connected to three planar 2-DOF movements in the base plane. A novel 6-DOF precision positioning table was presented in [27], which was assembled by two different 3-DOF precision positioning tables. A novel flexure based 6-DOF parallel positioning system for aligning the precision optical elements was presented by Kang et al[28]. A low stiffness 6-DOFcompliant precision stage was proposed in Ref. [29]. From the literature review, it is noted that the 6-DOF precision positioning systems can beconsidered as a system for combinations of in-plane and out-of-plane stages. However, based on the current manufacturing process technology

of precision positioning in micro/nano operating industry fields,the 6-DOF positioning system doesn't monolithically manufactured like as one-three-DOF positioning stages by wire electrical discharge machining technique. It means that manual assembly is needed.Therefore, in this paper, the proposed 6-DOF precision positioning system is assembled by two different 3-DOF precision positioning stages (as shown in Fig. 1). It has a simple structure and can easy beassembled, which significantly reduce the assembly errors and improve the system positioning accuracy.Such design strategy will improve the system stability and ensure that the system has good dynamic characteristics, rapidresponse and higher robustness against external disturbances.

In the past decade, different phenomeno-logicalhysteresis models have been established. Such as Preisach models [30, 31], Maxwell model[32], Duhem models [33], Bouc-Wen models [34-36], and Prandtl-Ishlinskii models [37]were developed to describe the hysteresis effect, which are then used to construct the inverse models for hysteresis compensation. It has already been verified that the Bouc-Wen model is suitable to describe the hysteresis loop of PEA [38]. In reference [39] the hysteresis nonlinearity was described by a dynamic backlash-like model. In order to improve the positioning accuracy, many controlmethodshave been proposed for tracking control of apiezoelectric-actuated nanopositioning stage.Feedforward controllers and feedback controllers wereused for the hysteresis and vibrationcompensation [40], respectively. Meanwhile, hybrid control is popular applied for high-precision control of piezo-actuated positioning stages, which combines the advantages of the feedforward

and feedback control. With such a control method, many works [41-44], have been recently reported and confirmed the feasibility of the control method for high-precision control of piezo-actuated positioning stages. However, there are some other control methods have been reported, such as proxy-based sliding-mode control [45].

This paper is organized as follows: Section 2 starts with the mechanical design of the 6-DOF positioning system. Section 3 provides the kinematic analysis of the system. In Section 4, FEA has been performed to investigate the static and dynamic characteristics of the 6-DOF system. Experimental setup and results have been provided in section 5. Finally, conclusions are presented in Section 6.

2. Mechanical design

Figure 1 shows the 3D solid model of a 6-DOF precision positioning system. It includes two main components, i.e. an in-plane 3-DOF positioning stage and an out-of-plane 3-DOF positioning stage.

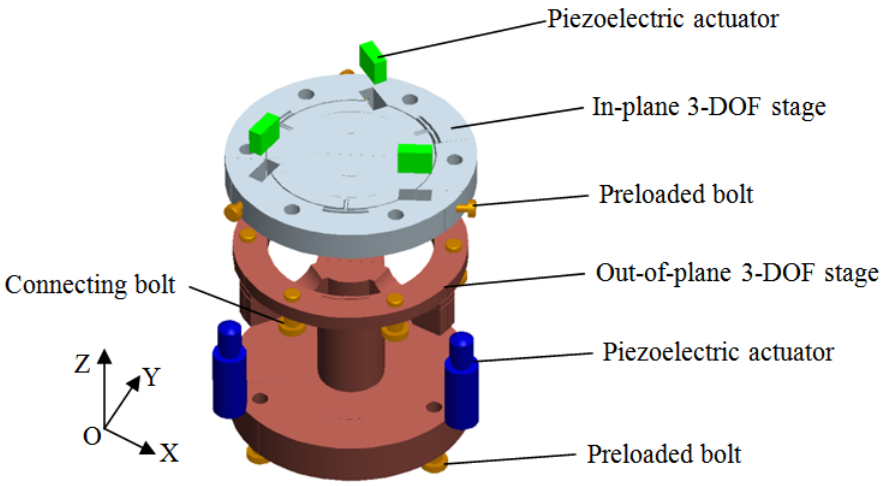

(a)

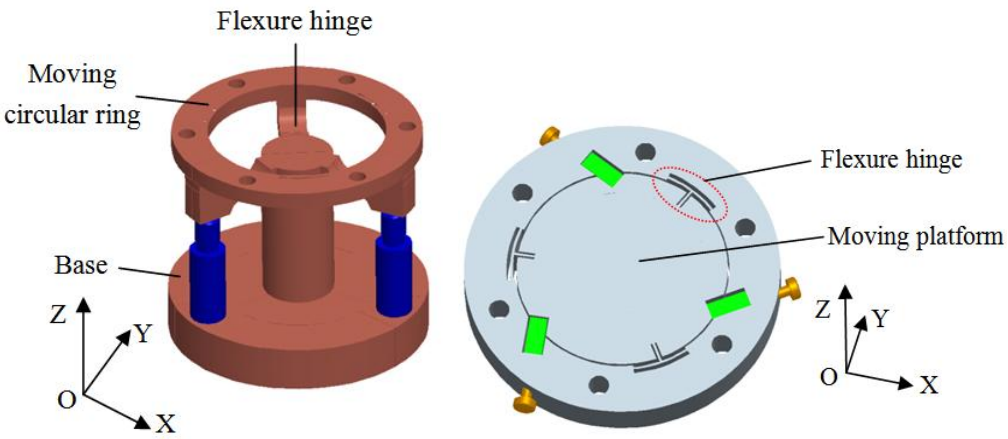

(b) (c)

Figure 1 3D solid model of the 6-DOF positioning system. (a) Exploded view, (b) the out-of-plane 3-DOF stage and (c) the in-plane 3-DOF stage

2.1 The design of the in-plane 3-DOF stage

The in-plane 3-DOF precision positioning stage is designed to realizethe X- and Y- axes translations and Z- axis rotation. As shown in Fig.2, the stage is mainly composed of three piezoelectric actuators(PEAs), three flexible mechanisms, amoving platform and a base. In the center of the moving platform, there are three grooves in the same circle with theseparated angle of 120°. Three PEAs are installed in these three grooves, and the end of each PEA is connected to the base by the preload bolt to ensure that the PEAs are fixed with the base and the moving platform is not separated during working condition. Three flexible mechanisms based on flexible hinges are arranged in the same circle with the grooves, with the separated angle of 120° between them and 60° with grooves, respectively. Each flexible mechanism is composed of three T-typeleaf-spring hinges,which is connected to the base and the moving platform at each end of the flexure hinge.

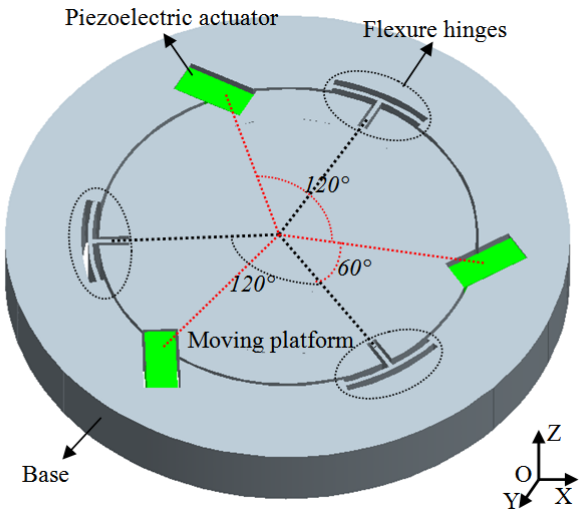

Figure 2 Mechanical structure of the in-plane 3-DOF stage.

As seen from Fig. 2, the structure of the in-plane stage is simple and compact by the symmetrical arrangement of the T-type flexure hinge mechanism. It is well-known that the performance of guide mechanism will determine the motion characteristics of the moving platform. Therefore, the performance of T-type flexible hinge mechanism needs be firstlyinvestigated. In order to investigate the performance of T-type flexible hinge mechanism, modal analysis is performed to examine its dynamic characteristics with finite element analysis (FEA) software (ANSYS Workbench). The material of the 3-DOF in-plane stagewas selected as Aluminum 7075-T6 with a Young's modulus of 72GPa, a yield strength in excess of 434MPa. The boundary conditions of simulation are setas thatthe outer edge of the both hinges I and II are fixed and constrained for all degrees offreedom, as shown in Fig. 3(a). The first three vibration mode shapes areobtained and shown in Fig. 3(b-d). It can be seen that only the leaf-spring hinge III generates an oscillate along the Y- axisfor the first mode shape; the second mode shapeis that the hingesI and II rotation about the Y- axis; and the third mode shapeis that the hinges I and II oscillate along the X- axis. In order to

guarantee the motion characteristics of the moving platform, the undesired motion must be avoided, such as the second modal, which can bring the instability of the stage.In addition, the modal analysis shows that the natural frequencies of T-type flexible hinge mechanism are high, enabling faster response and higher robustness against low-frequency disturbances. These will ensure that the system has better dynamic characteristics.

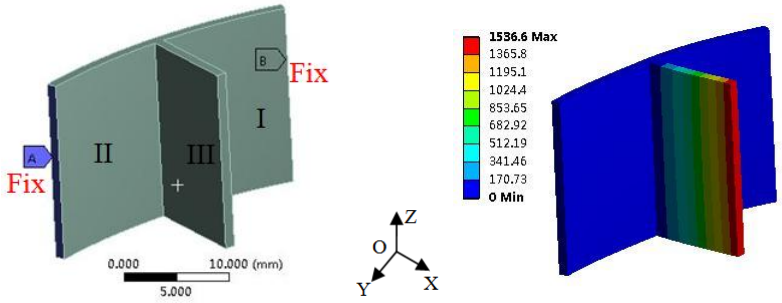

(a)

(b)

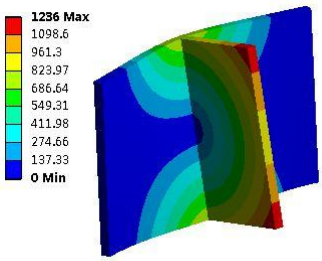

(c)

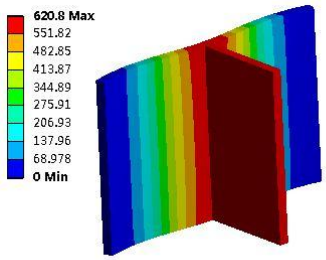

(d)

Figure 3 (a)The boundary conditions for simulation, (b) first mode shape (6199.6 Hz), (c) secondmodeshape (8722.2 Hz) and (d) thirdmodeshape (10197 Hz).

In order to further examine performance of the stage described above, the dynamic characteristics of the in-plane 3-DOF stage are investigatedand theresults are shown in Fig. 4. When the stage is not installed piezoelectric actuators, the first mode shape is the rotation about the Z-axis with the frequency of 528.11Hz; the second and

third modes shape are the translation along the Y-axis and X-axis, respectively, with the corresponding frequencies of 626.92Hz and 626.95 Hz, accordingly.

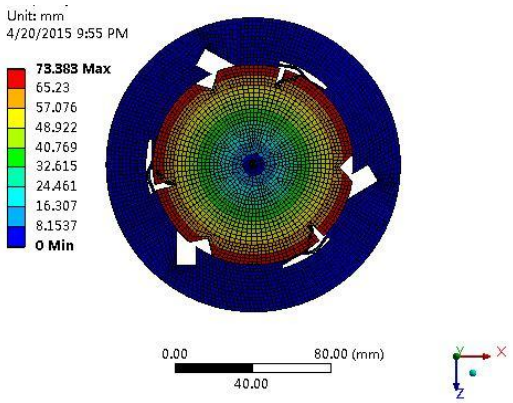

(a)

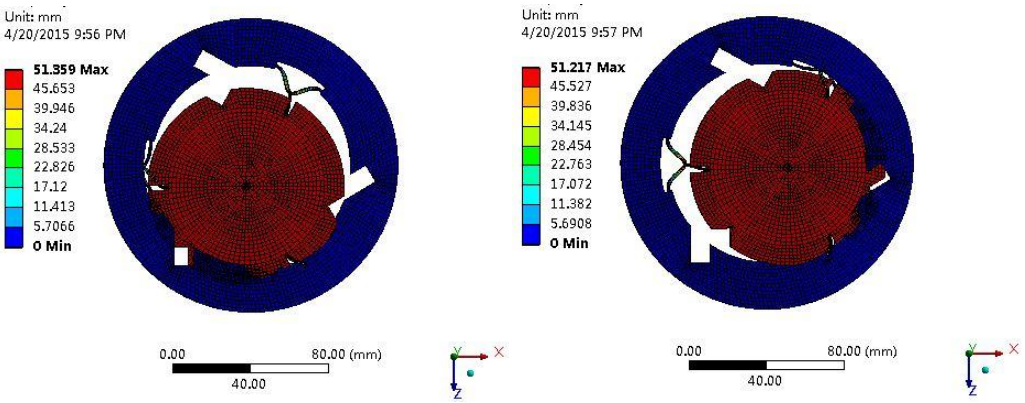

(b) (c)

Figure 4 First three mode shapes of the in-plane 3-DOF stage with no PEAs installed: (a) first modeshape (528.11Hz), (b) second mode shape (626.92Hz) and (c) third mode shape (626.95Hz).

According to the above characteristics analysis, it validates that the advantages of the design idea. The motion characteristicsof the special T-type hinge mechanism are more flexible, which can provide motion in two directions like thefirst and third mode shape in Fig. 3. In addition, the desired motions of the in-plane 3-DOF stage can be achieved, which can provide both translational and rotational motion characteristics. The motion and thermal stability of the stage will be improved by the

guide mechanism symmetrical arrangement. Furthermore, the in-plane stage has a high dynamic frequency, and these will ensure that the system has good dynamic characteristics.

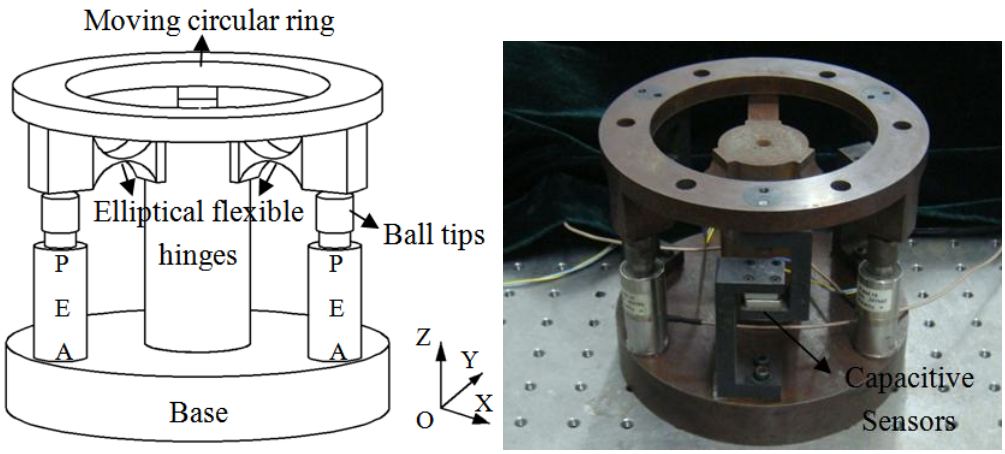

(a) (b)

Figure 5 (a) Schematicdiagram of the out-of-plane 3-DOF stage and (b) developed prototype

2.2 The design of the out-of-plane 3-DOF stage

The out-of-plane 3-DOF precision positioning stage is shown inFig. 5. The stage is mainly composed of three piezoelectric actuators, three elliptical flexible hinges, three high precision capacitivesensors, a moving circular ring and a base with central column. Three parallel piezoelectric actuators are securedwith axial symmetry around the circumference of acylindrical base and press against the elliptical flexible hinges through ball tips.The end of each PEA is connected to the base by the bolt preload to ensure that the PEAs are fixed with the base and the hingesare not separated during normal operations. Because of the brittle characteristic of piezoelectricmaterials, the actuators are strong enough against compressive force, but weak against shear force. The actuatorscannot supply lateral stiffness and are liable to be damaged from lateral

forces.To solve this problem, drive ball tips mounted onto theactuators push against the hinges under Hertzian contact conditions.Three elliptical flexure hinges connect the movingcircular ring to a central column. The hinges provide both alaterally stiff guidance mechanism for the moving circular ringand a spring preload for the PEAs. Three high precision capacitivesensors are used for the closed-loop displacement feedbackcontrol of the platform.The sensors are commercialparallel plate devices held on brackets between thecircular ring and the base in a symmetrical arrangement on thesame pitch-circle as the actuators.

The high-precision motion is generated by torsional deformation of theelliptical flexible hinges induced by PEAs, which is controlled by a computer. As shown in Fig. 6, elliptical flexure hinges are modeled as the revolutejoints with constant torsional stiffness, and the stiffness of the hinge is a major design parameter in the positioning system. Using the method presented by Qin [46], the detail of deflection formulae for an elliptical flexure hinge can be obtained. As shown in Fig. 6, definingthedeflectionvectoras $[\alpha_{zB}\ \Delta y_B\ \Delta x_B]^{\mathrm{T}}$and load vector as $[M_z\ F_y\ F_x]^{\mathrm{T}}$. The compliance matrix can be given as:

$$\begin{bmatrix} \alpha_{zB} \\ \Delta y_B \\ \Delta x_B \end{bmatrix} = \begin{bmatrix} P_1 & l_0 P_1 & 0 \\ l_0 P_1 & l_0^2 P_1 + P_2 & 0 \\ 0 & 0 & P_3 \end{bmatrix} \begin{bmatrix} M_z \\ F_y \\ F_x \end{bmatrix} \tag{1}$$

The detailed calculation process can be found in [46].

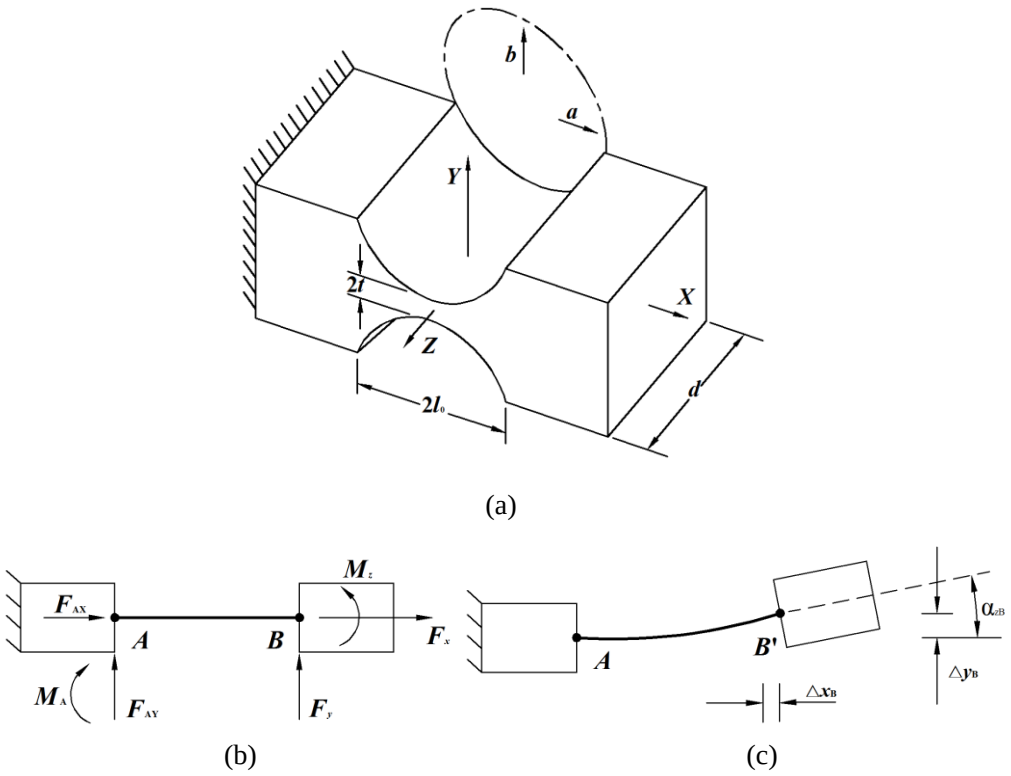

Figure 6 Geometric model of the elliptical flexure hinge. (a) Geometry and parameters; (b) loads and reactions; (c) deflections [46].

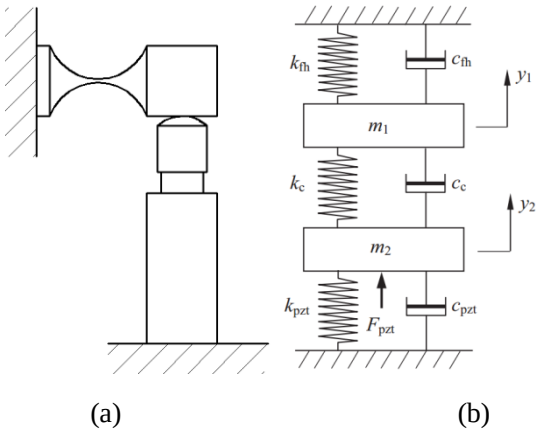

Figure 7 (a) Schematic diagram of the PEA press against the hinge through ball tipand (b) its simplified dynamic model

The PEAs press against the hinges through ball tips.The end of each PEA is connected to the base by the bolt preload to ensure that the PEAs are fixed with the base and the hinges are not separated during normal operation. As shown in Fig. 7(a),

the model of PEAs press against the hinges through ball tips. The displacement output of the free PEA is given by

$$d = d_{33}V \tag{2}$$

whered_{33} is a piezoelectric constant, and V is the applied voltage. From the dynamics point of view, the model can be considered as mass and spring system, as shown in Fig.7(b), $k_{pzt}$is the stiffness of PEA, k_c is the equivalent stiffness of Hertzian contact, which is related to the preload, k_{fh} is the equivalent stiffness in vertical direction of elliptical flexure hinge. Because of the presence of the hinge and preloading, the displacement output of the system is smaller than that of the free PEA. Thus, the steady-state displacement output of the system can be represented by

$$s = \frac{k_c k_{pzt}}{k_{fh}k_c + k_c k_{pzt} + k_{pzt}k_{fh}} d \tag{3}$$

After a preload is determined, displacement characteristics of the system are directly dependent on the output characteristics of the PEA. That is the output accuracy of PEA that will determine the positioning accuracy of the system.

Based on the second Newton's second law of motion, thedifferential equations for dynamic motion of the model are given as follows:

$$\begin{bmatrix} m_1 & 0 \\ 0 & m_2 \end{bmatrix}\begin{bmatrix} \ddot{y}_1 \\ \ddot{y}_2 \end{bmatrix}+\begin{bmatrix} c_{fh}+c_c & -c_c \\ -c_c & c_{pzt}+c_c \end{bmatrix}\begin{bmatrix} \dot{y}_1 \\ \dot{y}_2 \end{bmatrix}+\begin{bmatrix} k_{fh}+k_c & -k_c \\ -k_c & k_{pzt}+k_c \end{bmatrix}\begin{bmatrix} y_1 \\ y_2 \end{bmatrix}=\begin{bmatrix} 0 \\ F_{pzt} \end{bmatrix} \tag{4}$$

It is well known that a positioning system with a high naturalfrequency can be effectively against low-frequency disturbances and enabling faster response. These will ensure that the system has better dynamic characteristics. As previously mentioned, the flexure hinge is an important component of the system, and the natural

frequencies of the system have a close relation with the stiffness of the hinge. From equation (4), it is noted that *t* is a main factordeciding the stiffness of the hinge. Therefore, during the design, *a* and *b* are first determined according to the requirement of the design parameters. In addition, the hinges must be inside the small and compact stage, and all parameters should have values considering the stage size and arrangement. Furthermore, it should also consider the design specification of the displacement output of the system.

The novel 6-DOFprecision positioning system, as shown in Fig. 8, is assembled by two differentkinds of 3-DOF positioning stages, an in-plane stage and an out-of-plane stage. In such a combination system, the references [24] and [27] have proposed, both of them have designed that the in-plane 3-DOF stage located at the bottom of the 6-DOF system has to carry the out-of-plane 3-DOF stage, whichhave much larger masses than the specimen itself.This requiresthe in-plane stage has an excellent carrying capacity and uses much more powerful actuators, which is ineffective in energy consumption during normal operation. However, these design ideas affect the performance of a precision positioning system significantly. In addition, to the authors' knowledge, the present in-plane precision positioning stages have not been satisfactorycarrying capacity in generally. For the above reasons, this design idea is not suitable from viewpoints of both positioning accuracy and fast positioningresponse speed. In this proposed 6-DOF positioning system, the in-plane stage is mounted onthe top of the out-of-plane stage. Both two stages were manufactured monolithically using wire electricaldischarge machining (wire EDM)

technology, Al7076 T6 and springsteel 65Mn were adopted as the material of the in-plane and out-of-plane 3-DOF stage, respectively.Compared with the systems in references [24] and [27], the proposed system has the advantages of lighter moving mass,lower power consumption, smaller moving inertia and higher stability, which can ensure faster response speed and high-accuracy positioning.

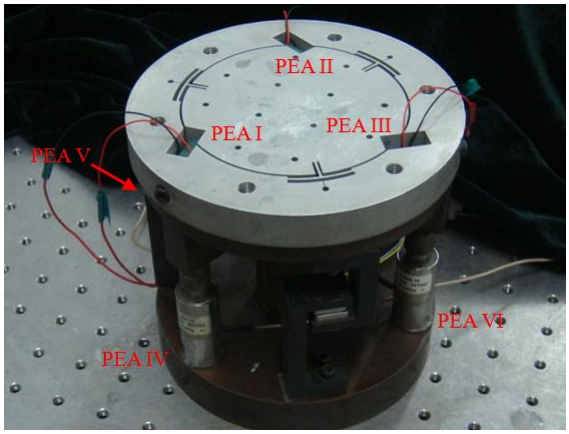

Figure 8 Manufactured prototype of 6-DOF positioning stage

3. Kinematic analysis of the 6-DOF positioning system

3.1 Kinematic model of the 3-DOF in-plane system

Figure 9 shows the geometry schematic diagram of the 3-DOF in-plane system.A_1, B_1 and C_1 are the contact points between the PEAs and the moving platform, and a geometric model of the stage can be simplified as a triangle ABC with three driving levers A-A_1, B-B_1 and C-C_1. As shown in Fig. 9(a), a reference coordinate O-XY is established. A moving coordinate O'-$X'Y'$ is established and shown in Fig. 9(b). In the coordinate O-XY, the coordinates of points O, A and A_1 are (0,0), (r, 0) and (r,-l), respectively. When the PEA drives the lever A-A_1, the position of the center O moves to O' whose coordinate is (x, y, α) and the points A and A_1 move to

points A' and A'_1, respectively.

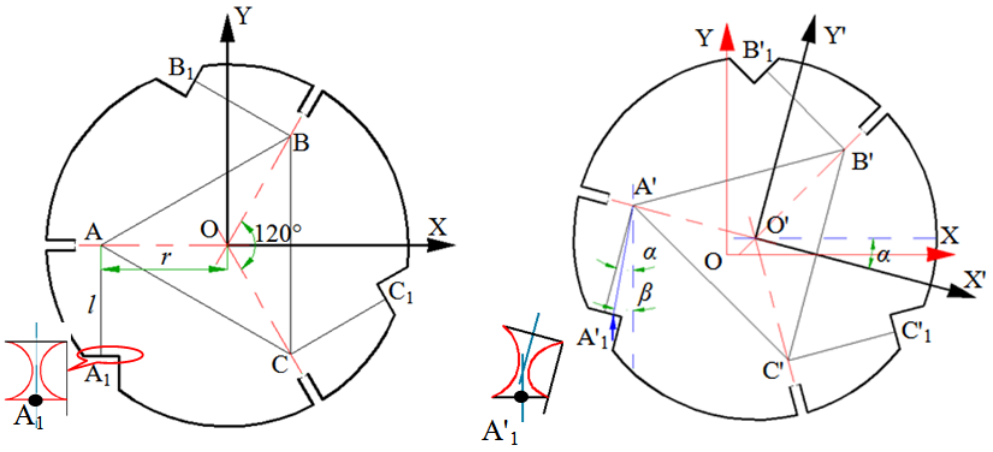

(a) (b)

Figure 9 Geometry schematic diagram of the moving platform.

As shown inFig. 9, a circular flexible hinge is used to model the contact between the PEA and the moving platform, and thus it can ensure that the PEA contacts with the moving platform during motion process, meanwhile allowing relatively rotation deformation between them.

The coordinate of points A' and A_1' in the coordinate$O$-XY, respectively:

$$(A'_x, A'_y) = (x + r\cos\alpha, y + r\sin\alpha) \quad (5)$$

$$(A'_{1x}, A'_{1y}) = (A'_x + l\sin\beta, A'_y - l\cos\beta) \quad (6)$$

Thus

$$A'_{1x} = A'_x + l\sin\beta = A_{1x} = r \quad (7)$$

And

$$\sin\beta = \frac{r - A'_x}{l} = \frac{r(1-\cos\alpha) - x}{l}$$

$$(A'_{1x}, A'_{1y}) = \{r, y + r\sin\alpha - \sqrt{l^2 - [r(1-\cos\alpha) - x]^2}\}$$

Therefore

$$\delta_{A'_1-A_1} = \left\|A'_1 - A_1\right\| = l + y + r\sin\alpha - \sqrt{l^2 - \left[r(1-\cos\alpha) - x\right]^2} \quad (8)$$

Similarly, the following equations are obtained:

$$\delta_{B'_1-B_1} = \left\|B'_1 - B_1\right\| = l + (-\frac{y}{2} - \frac{\sqrt{3}}{2}x) + r\sin\alpha - \sqrt{l^2 - \left[r(1-\cos\alpha) - (\frac{\sqrt{3}}{2}y - \frac{x}{2})\right]^2} \quad (9)$$

$$\delta_{C'_1-C_1} = \left\|C'_1 - C_1\right\| = l + (-\frac{y}{2} + \frac{\sqrt{3}}{2}x) + r\sin\alpha - \sqrt{l^2 - \left[r(1-\cos\alpha) - (-\frac{\sqrt{3}}{2}y - \frac{x}{2})\right]^2} \quad (10)$$

Thus

$$\begin{bmatrix} \delta_{A'_1-A_1} \\ \delta_{B'_1-B_1} \\ \delta_{C'_1-C_1} \end{bmatrix} = \boldsymbol{T}_{in} \begin{bmatrix} x \\ y \\ \alpha \end{bmatrix} \quad (11)$$

And

$$\boldsymbol{T}_{in} = \begin{bmatrix} \frac{\partial(\delta_{A'_1-A_1})}{\partial x} & \frac{\partial(\delta_{A'_1-A_1})}{\partial y} & \frac{\partial(\delta_{A'_1-A_1})}{\partial \alpha} \\ \frac{\partial(\delta_{B'_1-B_1})}{\partial x} & \frac{\partial(\delta_{B'_1-B_1})}{\partial y} & \frac{\partial(\delta_{B'_1-B_1})}{\partial \alpha} \\ \frac{\partial(\delta_{C'_1-C_1})}{\partial x} & \frac{\partial(\delta_{C'_1-C_1})}{\partial y} & \frac{\partial(\delta_{C'_1-C_1})}{\partial \alpha} \end{bmatrix} \quad (12)$$

The initial value (0,0,0) is substituted into equation (12), therefore

$$\frac{\partial(\delta_{A'_1-A_1})}{\partial x}\Big|_{(0,0,0)} = 0 \quad \frac{\partial(\delta_{A'_1-A_1})}{\partial y}\Big|_{(0,0,0)} = 1 \quad \frac{\partial(\delta_{A'_1-A_1})}{\partial \alpha}\Big|_{(0,0,0)} = r$$

$$\frac{\partial(\delta_{B'_1-B_1})}{\partial x}\Big|_{(0,0,0)} = -\frac{\sqrt{3}}{2} \quad \frac{\partial(\delta_{B1'-B1})}{\partial y}\Big|_{(0,0,0)} = -\frac{1}{2} \quad \frac{\partial(\delta_{B'_1-B_1})}{\partial \alpha}\Big|_{(0,0,0)} = r$$

$$\frac{\partial(\delta_{C'_1-C_1})}{\partial x}\Big|_{(0,0,0)} = \frac{\sqrt{3}}{2} \quad \frac{\partial(\delta_{C'_1-C_1})}{\partial y}\Big|_{(0,0,0)} = -\frac{1}{2} \quad \frac{\partial(\delta_{C'_1-C_1})}{\partial \alpha}\Big|_{(0,0,0)} = r$$

The relationship between output displacement and input displacement can be expressed as

$$\begin{bmatrix} x \\ y \\ \alpha \end{bmatrix} = \boldsymbol{T}_{in}^{-1} \begin{bmatrix} \delta_{A'_1-A_1} \\ \delta_{B'_1-B_1} \\ \delta_{C'_1-C_1} \end{bmatrix} \tag{13}$$

And, the transformation matrix$\boldsymbol{T}^{-1}_{in}$can be obtained as follows:

$$\boldsymbol{T}_{in}^{-1} = \begin{bmatrix} 0 & \frac{1}{\sqrt{3}} & -\frac{1}{\sqrt{3}} \\ \frac{2}{3} & -\frac{1}{3} & -\frac{1}{3} \\ \frac{1}{3r} & \frac{1}{3r} & \frac{1}{3r} \end{bmatrix} \tag{14}$$

3.2 Kinematic model of the 3-DOF out-of-plane system

Figure 10 shows the geometry schematic diagram of the locations, P_i(i=4,5,6) of the piezoelectric actuators relative to the movingcircular ring. According to the space geometric relationship, the following relationship can be obtained:

$$\begin{cases} z = \dfrac{\delta_4 + \delta_5 + \delta_6}{3} \\ \sin\theta_y = \dfrac{2\delta_6 - (\delta_4 + \delta_5)}{3R} \\ \sin\theta_x = \dfrac{\delta_4 - \delta_5}{\sqrt{3}R} \end{cases} \tag{15}$$

where$\theta_x$and $\theta_y$arethe angle rotation about the X and Y-axes of the coordinate system*O-XY*, respectively.δ_4, δ_5, δ_6 arethe elongation of the PEAs in the 3-DOF stage. Considering the rotation angle are very small (only130μrad), the equation (15) can be written as follows:

$$\begin{bmatrix} z \\ \theta_y \\ \theta_x \end{bmatrix} = \frac{1}{3} \begin{bmatrix} 1 & 1 & 1 \\ 2/R & -1/R & -1/R \\ 0 & \sqrt{3}/R & -\sqrt{3}/R \end{bmatrix} \begin{bmatrix} \delta_6 \\ \delta_5 \\ \delta_4 \end{bmatrix} \tag{16}$$

Thus, the transformation matrix$\boldsymbol{T}^{-1}_{out}$can be obtained as follows:

$$\boldsymbol{T}_{out}^{-1}=\begin{bmatrix}\frac{1}{3} & \frac{1}{3} & \frac{1}{3}\\ \frac{2}{3R} & -\frac{1}{3R} & -\frac{1}{3R}\\ 0 & \frac{\sqrt{3}}{3R} & -\frac{\sqrt{3}}{3R}\end{bmatrix} \tag{17}$$

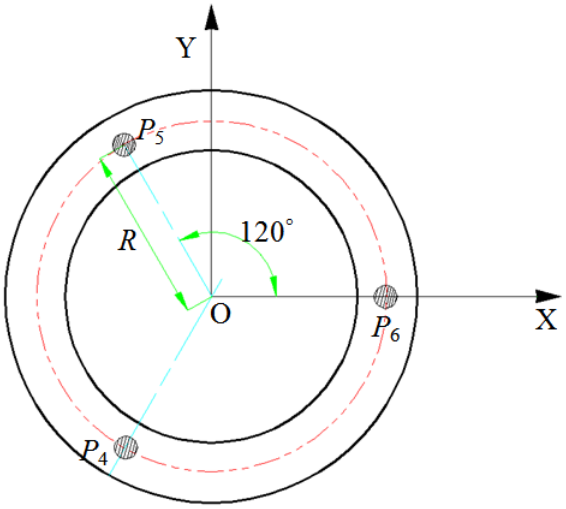

Figure 10 Themoving circular ring and locations of the actuators

3.3 The transformation matrix of the 6-DOF positioning system

In order to describe the kinematic analysis of the 6-DOF positioning system, the transformation matrix $\boldsymbol{T}^{-1}$ is presented. The 6-DOF positioning system can achieve only one- or multi-direction positioning by six PEAs with different output displacements. Referring to equation (18), the transformation matrix $\boldsymbol{T}^{1}$ between the input displacements matrix $\boldsymbol{I}$ and output displacements matrix $\boldsymbol{O}$ can be expressed as

$$\boldsymbol{O} = \boldsymbol{T}^{-1} \times \boldsymbol{I} \tag{18}$$

where,$\boldsymbol{O}=[x\ y\ \alpha\ \theta_x\ \theta_y z]^{\mathrm{T}}$, $\boldsymbol{I}=[\delta_1\ \delta_2\ \delta_3\ \delta_4\ \delta_5 \delta_6]^{\mathrm{T}}$.$\delta_1$, δ_2, and $\delta_3$arethe elongation of the PEAs in the in-plane stage, and δ_4, δ_5, and δ_6 arethe elongation of the PEAs in the out-of-planestage, respectively; x, y, z and α, θ_x, $\theta_y$arethe displacements in the X-, Y-,

Z-axes and the rotation angles about the*Z*-, *X*-, *Y*-axes of the moving platform, respectively.

This transformation matrix provides a useful tool to predict the relationship between output displacement of the system and the amountof expansion of PEAs. Then multi-group and random input displacements are inputted, andthe impact of the cross-coupling of the system must be considered. In order to obtain the transformation matrices $\boldsymbol{T}^{-1}$, the analysis model should be proposed as follow.

According to the geometricalrelation, as shown in Fig. 11, a reference coordinate *O*-*XYZ*is established. A moving coordinateO_d-$X_dY_dZ_d$ is located at the center of the movingcircular ring on the out-plane 3-DOF stage, which coincides with the fixed reference coordinate *O*-*XYZ*.The other coordinate frame O_s-$X_sY_sZ_s$is located at the center of the moving platform ofthe 3-DOF in-plane system.

It is noted that the moving coordinateO_d-$X_dY_dZ_d$ relative to the reference coordinate *O*-*XYZ* has been rotated byθ_x, θ_y around the *X*- and *Y*-axis, and translated by P_z along the *Z*-axis, respectively. The transformation matrix $\boldsymbol{T}_d$ can be represented by

$$\boldsymbol{T}_d = R(x,\theta_x)R(y,\theta_y)Tran\ (z,P_z) \tag{19}$$

Similarly, the moving coordinate O_s-$X_sY_sZ_s$ relative to the coordinate O_d-$X_dY_dZ_d$ has been translated by P_x,P_x and $T_z$along the *X*-, *Y*- and *Z*-axis, respectively, and rotated by α around the *Z*-axis. Thus, the transformation matrix $\boldsymbol{T}_{sd}$ of the moving coordinate O_s-$X_sY_sZ_s$ relative to the coordinate O_d-$X_dY_dZ_d$ can be obtained as follows:

$$\boldsymbol{T}_{sd} = Tran\ (x,P_x)Tran\ (y,P_y)Tran\ (z,T_z)R(z,\alpha) \tag{20}$$

Therefore, the transformation matrix $\boldsymbol{T}_s$ of the moving coordinate O_s-$X_sY_sZ_s$ relative to the reference coordinate O-XYZ can be obtained as follows:

$$\boldsymbol{T}_s = \boldsymbol{T}_d \boldsymbol{T}_{sd} \quad (21)$$

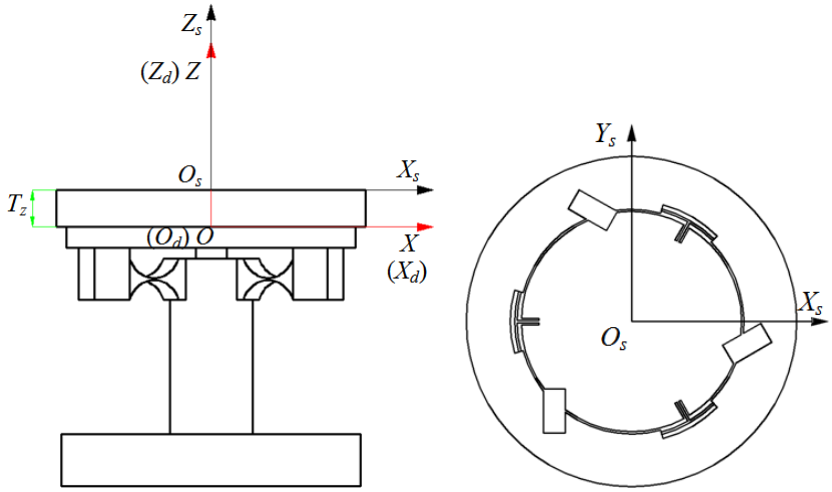

(a) Front view (b) Top view

Figure 11 Geometric model of the 6-DOF system

Therefore,

$$\boldsymbol{T}_s = \begin{bmatrix} g\theta_x g\theta_y & -e\theta_x g\theta_y & e\theta_y & P_x g\theta_y + T_z e\theta_y \\ e\theta_x e\theta_y e\alpha + g\theta_x e\alpha & -e\theta_x e\theta_y e\alpha + g\theta_x g\alpha & -e\theta_x g\theta_y & P_x e\theta_x e\theta_y + P_y g\theta_x - T_z e\theta_x g\theta_y \\ -g\theta_x e\theta_y g\alpha + e\theta_x e\alpha & g\theta_x e\theta_y e\alpha + e\theta_x g\alpha & g\theta_x g\theta_y & -P_x g\theta_x e\theta_y + P_y e\theta_x + T_z g\theta_x g\theta_y + P_z \\ 0 & 0 & 0 & 1 \end{bmatrix}$$

where$e=sin$,$g=cos$.Then, the displacement of the origin point O_s of O_s-$X_sY_sZ_s$ relative to the reference coordinate O-XYZ can be written as follows:

$$\begin{bmatrix} x \\ y \\ z \end{bmatrix} = \begin{bmatrix} P_x g\theta_y + T_z e\theta_y \\ P_x e\theta_x e\theta_y + P_y g\theta_x - T_z e\theta_x g\theta_y \\ -P_x g\theta_x e\theta_y + P_y e\theta_x + T_z g\theta_x g\theta_y + P_z \end{bmatrix} \quad (22)$$

Owing tosmall values of $\theta_x$and θ_y, it can be deduced that$sin\theta_x(\theta_y)\approx\theta_x(\theta_y)$, $cos\theta_x(\theta_y)\approx1$. Meanwhile, infinitesimal of higher orders are neglected. Therefore, the equation(22) can be written as

$$\begin{cases} P_x = x - \theta_y T_z \\ P_y = y + \theta_x T_z \\ P_z = z \end{cases} \tag{23}$$

According to the kinematicanalysis model of the in-plane and out-of-plane 3-DOF systems, the result can be obtained

$$\begin{cases} P_x = \dfrac{1}{\sqrt{3}}(\delta_2 - \delta_3) \\ P_y = \dfrac{1}{3}(2\delta_1 - \delta_2 - \delta_3) \\ P_z = \dfrac{1}{3}(\delta_4 + \delta_5 + \delta_6) \end{cases} \tag{24}$$

Therefore, the relation can be obtained

$$\begin{bmatrix} 0 & \frac{1}{\sqrt{3}} & -\frac{1}{\sqrt{3}} & 0 & 0 & 0 \\ \frac{2}{3} & -\frac{1}{3} & -\frac{1}{3} & 0 & 0 & 0 \\ \frac{1}{3r} & \frac{1}{3r} & \frac{1}{3r} & 0 & 0 & 0 \\ 0 & 0 & 0 & -\frac{\sqrt{3}}{3R} & \frac{\sqrt{3}}{3R} & 0 \\ 0 & 0 & 0 & \frac{1}{3R} & \frac{1}{3R} & -\frac{2}{3R} \\ 0 & 0 & 0 & \frac{1}{3} & \frac{1}{3} & \frac{1}{3} \end{bmatrix} \begin{bmatrix} \delta_1 \\ \delta_2 \\ \delta_3 \\ \delta_4 \\ \delta_5 \\ \delta_6 \end{bmatrix} = \begin{bmatrix} 1 & 0 & 0 & 0 & -T_z & 0 \\ 0 & 1 & 0 & T_z & 0 & 0 \\ 0 & 0 & 1 & 0 & 0 & 0 \\ 0 & 0 & 0 & 1 & 0 & 0 \\ 0 & 0 & 0 & 0 & 1 & 0 \\ 0 & 0 & 0 & 0 & 0 & 1 \end{bmatrix} \begin{bmatrix} x \\ y \\ \alpha \\ \theta_x \\ \theta_y \\ z \end{bmatrix} \tag{25}$$

And then, the transformation matrices $\boldsymbol{T}^{-1}$can be expressed as follows:

$$\boldsymbol{T}^{-1} = \begin{bmatrix} 0 & \frac{1}{\sqrt{3}} & -\frac{1}{\sqrt{3}} & \frac{T_z}{3R} & \frac{T_z}{3R} & -\frac{2T_z}{3R} \\ \frac{2}{3} & -\frac{1}{3} & -\frac{1}{3} & \frac{T_z}{\sqrt{3}R} & -\frac{T_z}{\sqrt{3}R} & 0 \\ \frac{1}{3r} & \frac{1}{3r} & \frac{1}{3r} & 0 & 0 & 0 \\ 0 & 0 & 0 & -\frac{\sqrt{3}}{3R} & \frac{\sqrt{3}}{3R} & 0 \\ 0 & 0 & 0 & \frac{1}{3R} & \frac{1}{3R} & -\frac{2}{3R} \\ 0 & 0 & 0 & \frac{1}{3} & \frac{1}{3} & \frac{1}{3} \end{bmatrix} \tag{26}$$

4 Finite element analysis

FEA is conducted to investigate the characteristics of the 6-DOF positioning system using ANSYS software, and the finite element model is shown in Fig. 12.

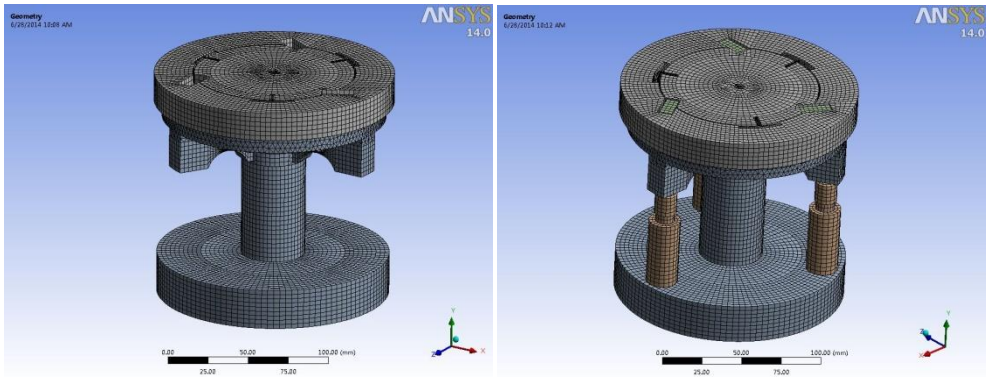

(a)(b)

Figure 12 Finite element model of the 6-DOF system: (a) without PEAs (b) with PEAs

4.1 Static Characteristic

In order to obtain the motion characteristics of the working area on the moving platform, the static characteristic analysis is carried out. As previously mentioned,because of the presence of preloading, the deformation and output displacement of the 6-DOF positioning system are obtained, which are shown in Figs. 13 and 14. There exists rotation error about the*Z*- axis when the moving platformmoves along the *Z*- axis.

The different working style of the drivingPEAs and the analysis results are shown in Figure 15. Fig. 15(a) shows that when only PEA IV works, the working area of the movable platform will rotate around the *X*-axis. Fig. 15(b) shows that when three PEAs(I, II and III) work together, the working area has onlypure rotation about the *Z*-axis. In Figure 15(c), it shows that when four PEAs(I, II,III and V) work

together, the working area has rotation about one axis which deviates from the Z-axis, due to the role of the PEA V. From the above analysis, it can be seen that the motion of the 6-DOF positioning system is coupled.

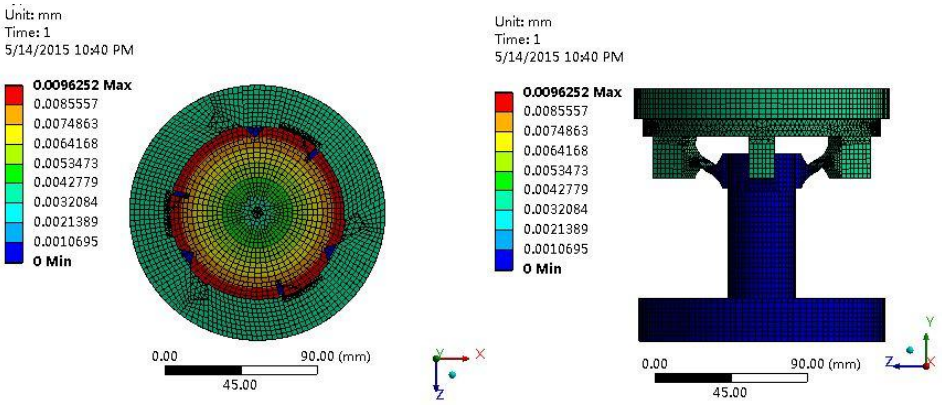

(a) Top view (b) Frontview

Figure 13 The deformation of the 6-DOF positioning system under the preload forces

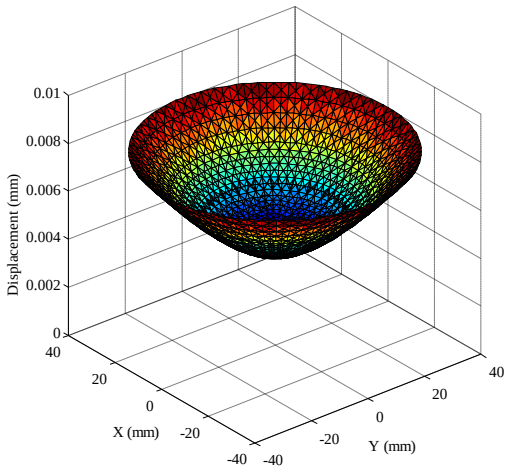

Figure 14 The displacement of the working area under the bolt preload

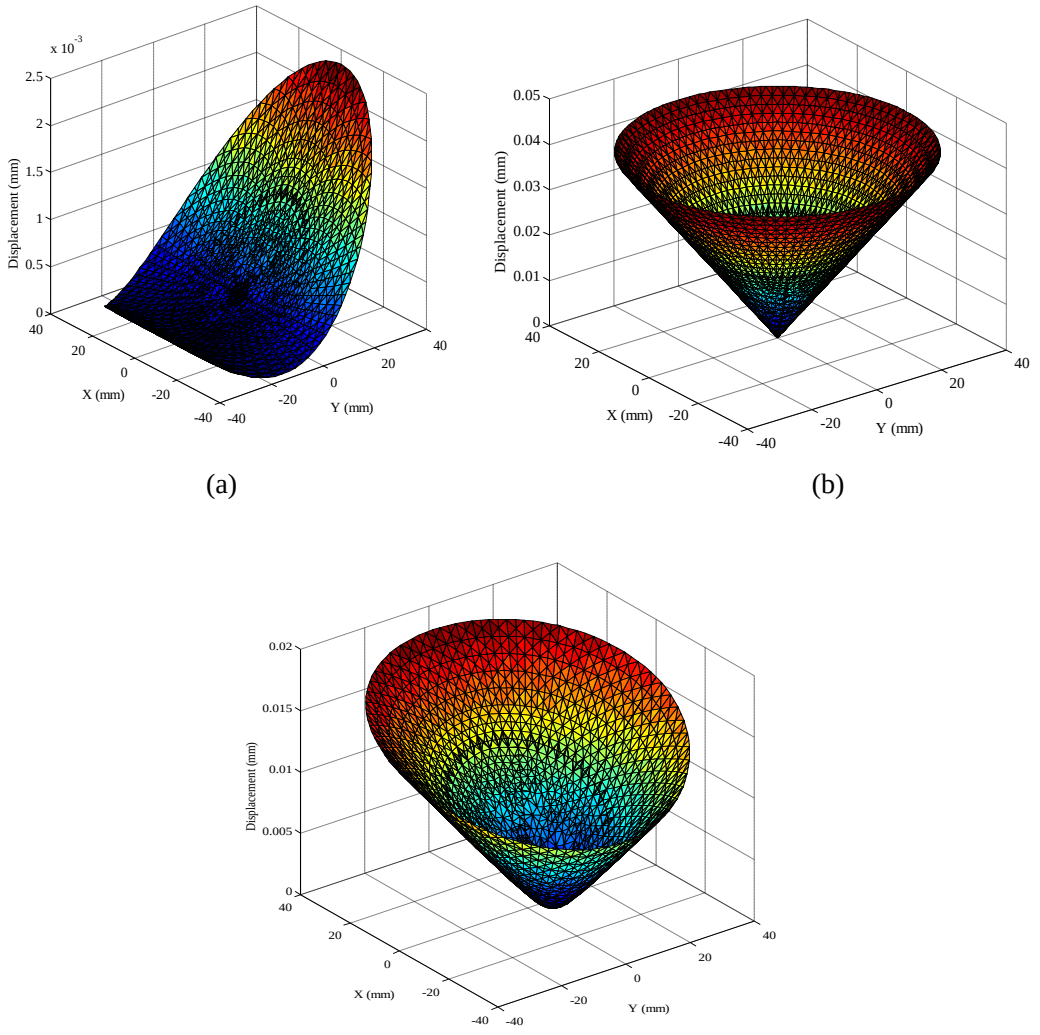

Figure 15 The displacement of the working area: (a) PEA IV works only, (b) PEA I, II and III work together and (c) PEA I, II, III and V work together.

Through data processing of the FEAresult, we can obtain the transformation matrix$\boldsymbol{T}^1$ as follow:

$$T^{-1} = \begin{bmatrix} 0.001 & -0.6283 & 0.6271 & 0.2166 & -0.4555 & 0.2385 \\ -0.7255 & 0.3611 & 0.3641 & -0.4017 & 0.0129 & 0.3885 \\ -6.015\times10^{-4} & -5.951\times10^{-4} & -5.956\times10^{-4} & 1.3\times10^{-5} & 1.2\times10^{-5} & 1.25\times10^{-5} \\ 1.8184\times10^{-6} & -3.4386\times10^{-7} & 5.5732\times10^{-6} & 0.32351 & 0.32236 & 0.32413 \\ -9.5\times10^{-6} & 5.5\times10^{-5} & -4.4\times10^{-5} & -2.9\times10^{-4} & 5.8\times10^{-4} & -2.9\times10^{-4} \\ -5.5\times10^{-5} & 1.9\times10^{-5} & 3.5\times10^{-5} & -5\times10^{-4} & 4\times10^{-6} & 5\times10^{-4} \end{bmatrix}$$

4.2 Dynamic Characteristic

The dynamic characteristics of the 6-DOF positioning system are investigated through modal analysis and the results are shown in Fig. 16. It shows the first eight mode shapes of the system with PEAs installed. The corresponding frequencies of the modes are shown in Table I. It is noted that the first three mode shapes illustrate that the moving platform rotates about the *X*-, *Y*- and *Z*- axis, respectively. The moving platform moves along the *Z*-axis in the fourth mode shape. In the fifth andsixth vibration mode shapes the moving platform rotates about the *X*- and *Y*-axis, respectively, and the three PEAs (IV, V and VI) are produced swing at the same time. In the seventh and eighth vibration modes the moving platform moves along the *X*- and *Y*-axis, respectively.

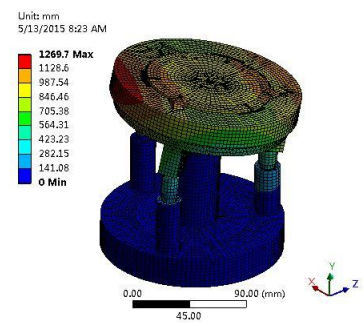

(1st)

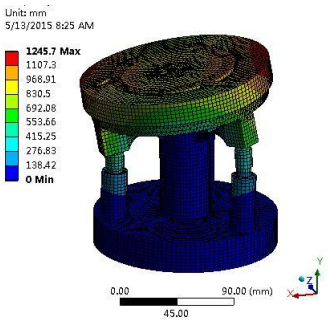

(2nd)

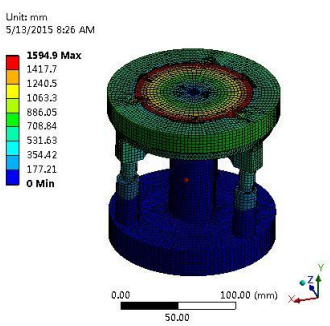

(3rd)

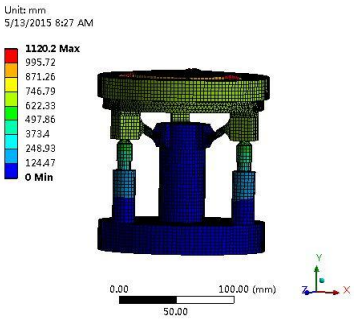

(4st)

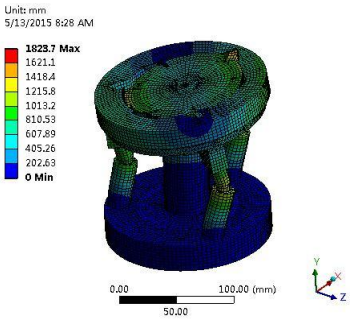

(5st)

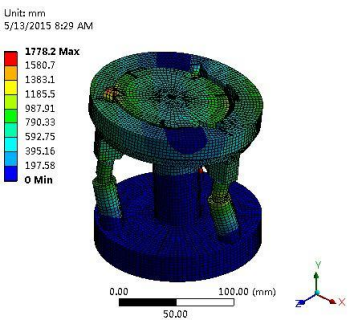

(6st)

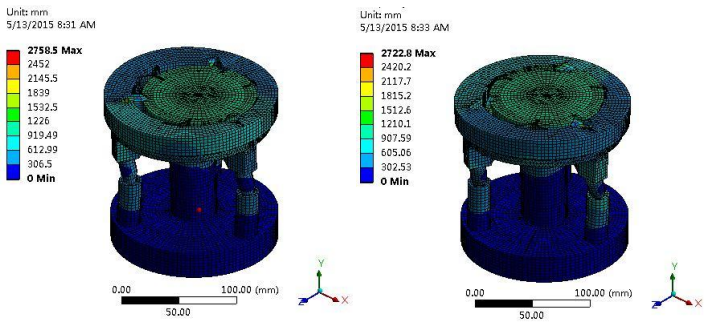

(7^{st}) (8^{st})

Figure 16 First eight mode shapes of the 6-DOF positioning system

Table I: The corresponding frequencies of the mode shapes.

Order	1^{st}	2^{nd}	3^{rd}	4^{st}
Frequency(Hz)	560.63	561.08	581.82	824.18
Order	5^{st}	6^{st}	7^{st}	8^{st}
Frequency(Hz)	1139.7	1140.2	1754.2	1754.6

According to the above characteristic analysis, it validates that the stage can provide 6 degree-of-freedom motions. In addition, the stage has a high natural frequency, which ensures that the system has good dynamic characteristics.

5. Experiment and Results

The performance of the proposed 6-DOF positioning system was systematically evaluated. As shown in Fig. 17(a), three AE0505D18 and three PI P-844.10 PEAs were used with the maximum displacement of 15μm under the input voltage of 100V, which were used to actuate the in-plane stage and out-of-plane stage, respectively. The dSPACE DS1103 controller was used to generate the controlling signal, the PI E-505.00 amplifier and 3-Axls Piezo Controller THORLABS MDT693B were used to amplify the signal then drive the PEAs. Three KEYENCE laser displacement sensors LK-H050 and three capacity position sensors D-050.00were used to measure the

motion of the in-plane and out-of-plane stage, respectively. The amplifier E-509.C3A for capacity position sensors was installed in a chassis.As described in Fig. 17(b). Frequency response measurements were carried out to evaluate the dynamic characteristics of the 6-DOF system. A hammer (IH-05) was used to apply excitation to the system; the response signal was measured by a 3-axis accelerometers (Brüel & Kjær 4506B) mounted on the moving platform. The data acquisition and analysis were performed using a modal analyzer (Brüel & Kjær 3050-B-6/0).

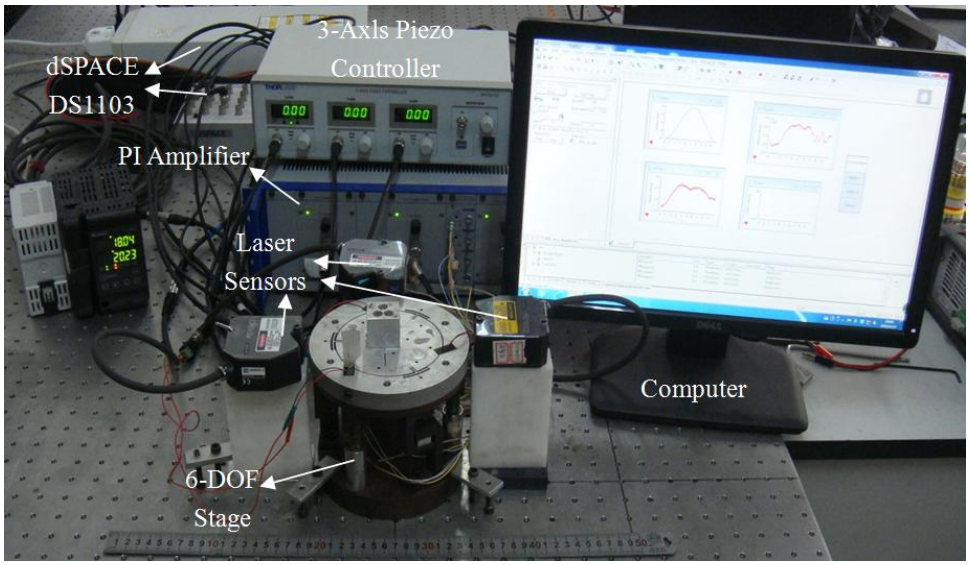

(a)

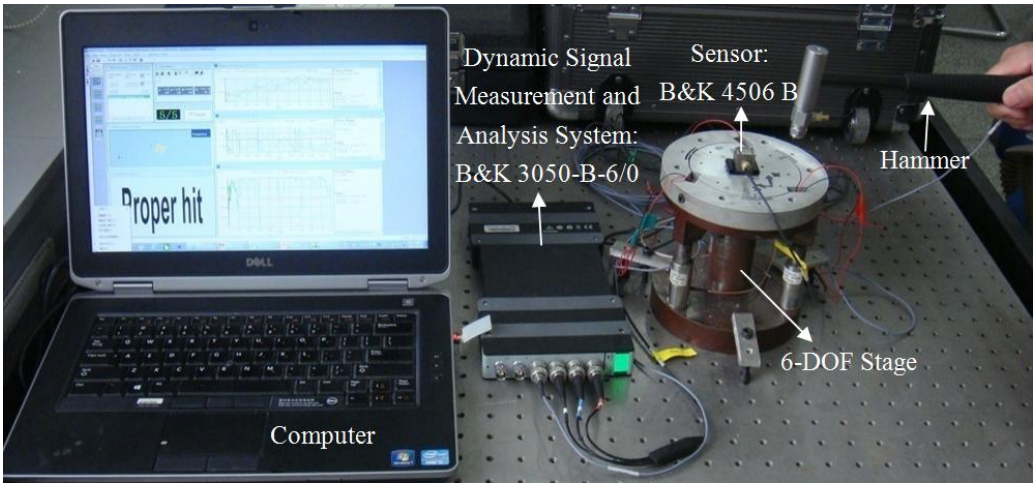

(b)

Figure 17 Experimental setup of the system: (a) Motion response, and (b) vibration testing.

Figure18 shows the Frequency Response Functions (FRFs) of the 6-DOF system. It can be found that the resonance frequency of the system is measured in the *X*, *Y* and *Z* direction, respectively, which are slightly larger than the simulation results.This result appearsfor several reasons, including the manufacturing errors, the bolt preload, and installation errors. It can be seen in Fig. 18 that the design structure provides thehigh dynamic bandwidth with the lowest resonant frequency of 585.6Hz.

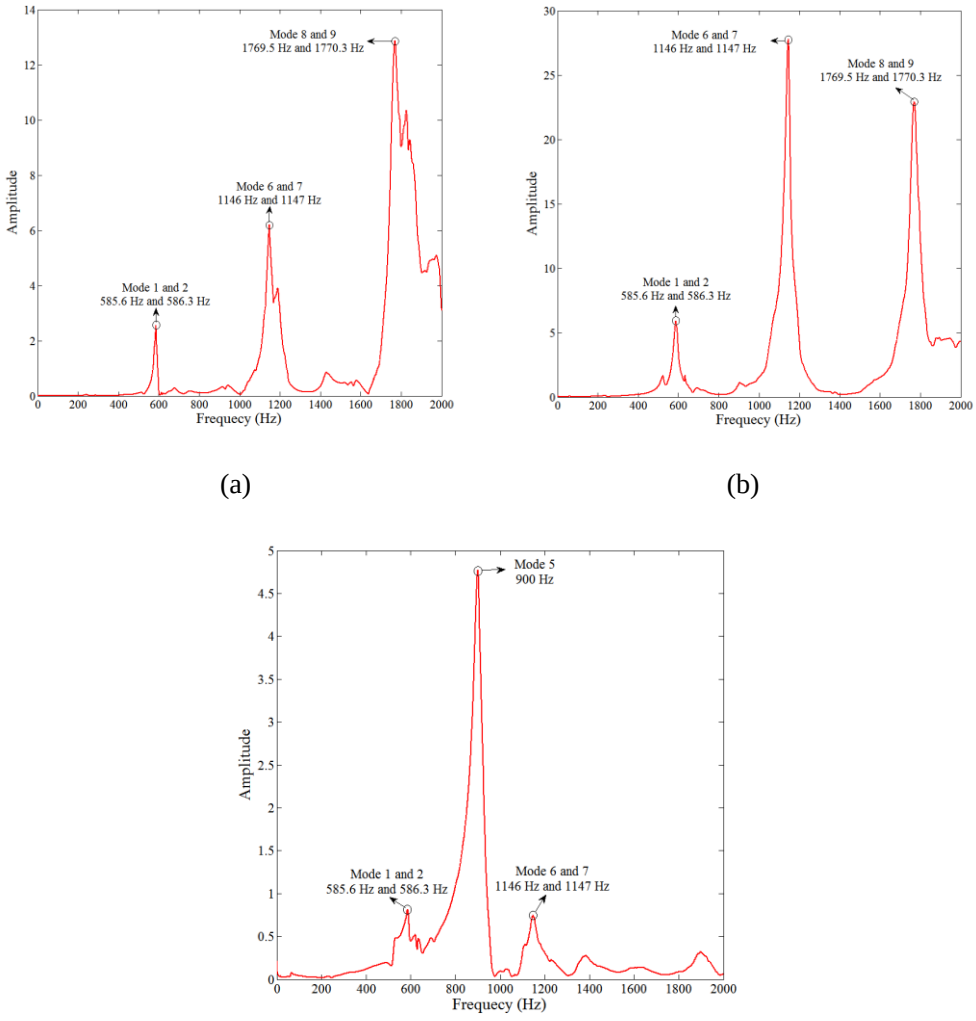

(a) (b)

(c)

Figure 18 Frequency Response Functions of the system: (a) Measured in the *X* direction, (b) Measured in the *Y* direction, (c) Measured in the *Z* direction.

5.1 Motion stroke and step responses

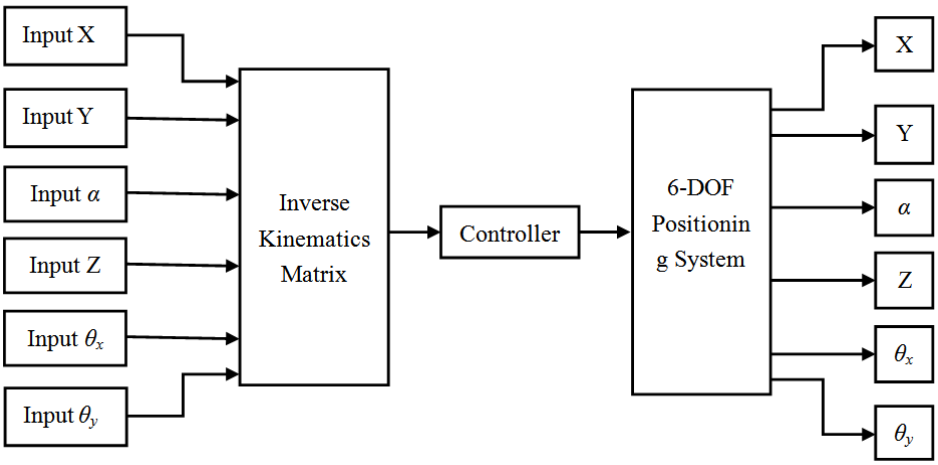

Figure 19 Open-loop decoupling control block diagram

As mentionedpreviously, the motion of the 6-DOF system is coupled. In order to eliminate this shortcoming, the system is controlled in open-loop via inverse kinematics. The control block diagram is presented in Fig.19. Therefore, each axis output of the system can be controlled independently when the system is controlled by the simultaneous actuation of the six PEAs. In this case, the 6-DOF system, which is controlled in open-loop via inverse kinematics, can be treated as six Single-Input-Single-Output (SISO) systems, and the cross-axis couplings can be treated as external disturbances. The inverse kinematic matrix is an inverse form of the matrix $\boldsymbol{T}^{-1}$ in the section 3.This will make it more convenient applied to the future work.

The step responses of the system are investigated, and the step responses in the *X*-, *Y*- and *Z*- axes directions are shown in Fig. 20. The result shows that the 2% settling time of the step responses are 38, 46 and 62 ms, respectively. The motion stroke is also measured and shown in Fig. 21. It is noted that the 6-DOF system has an

effective workspace of 8.2 μm× 10.5 μm× 13.0 μm× 224 μrad × 105 μrad × 97 μrad.

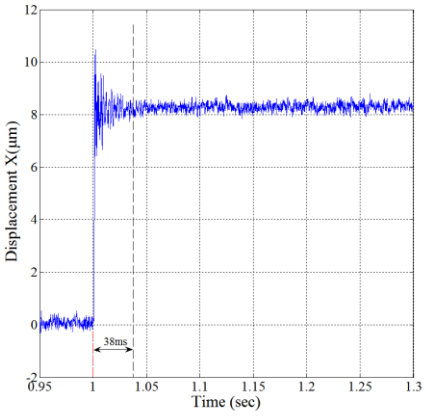

(a)

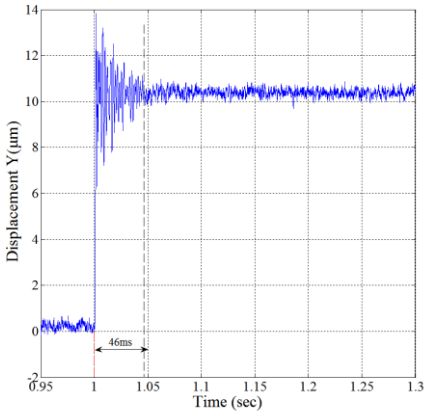

(b)

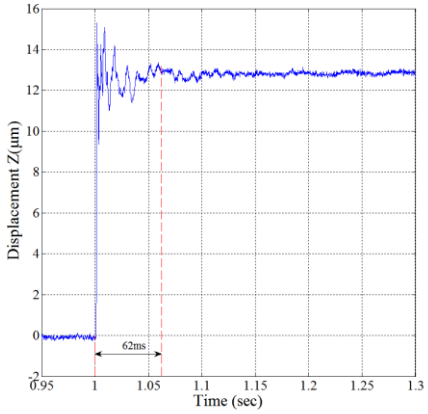

(c)

Figure 20 X-, Y- and Z- axes step responses (2% settling time).

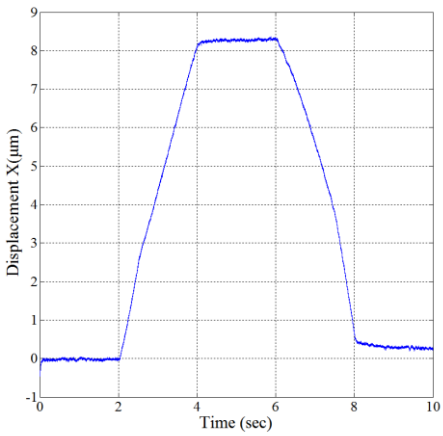

(a)

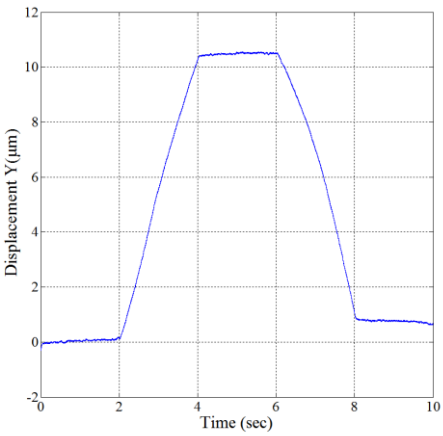

(b)

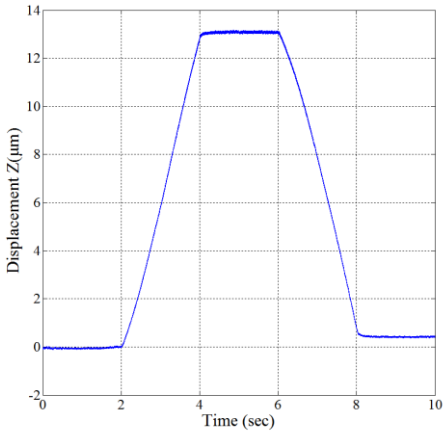

(c)

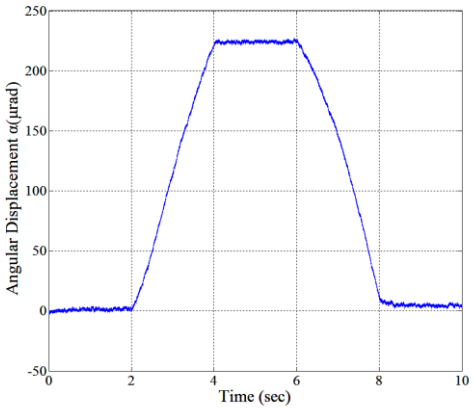

(d)

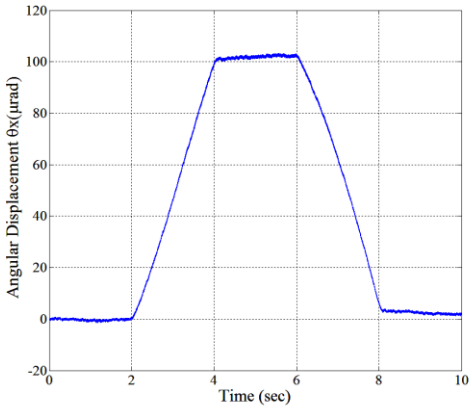

(e)

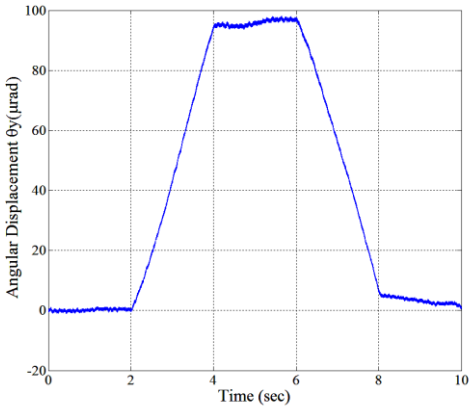

(f)

Figure 21 Experiment test of the motion stroke.

5.2 Trajectory tracking

During operations, the control voltage applied on the PEA, which is defined as theinput into the system, due to the hysteresis and creep effects of the PEA, the relationship between the input control voltage and the output displacement of the PEA is nonlinear.With respect to this hysteresis phenomenon, many hysteresis models have been developed to describethe hysteresis nonlinearities such as Preisach model[30,31], Maxwell model[32], Duhem model[33], Bouc-Wen model[34-36], Prandtl-Ishlinskii

model[37]. In this paper, the Bouc-Wen hysteresis modelis selected as an illustration. Certainly, other hysteresis modelscan also be selected. Without loss of generality, it has already been verified that the Bouc-Wen model is suitable to describe the hysteresis loop of PEA [38]. The equation of a B-W model is shown as follows:

$$\dot{h} = ad_e\dot{V}_{pzt} - b\left|\dot{V}_{pzt}\right|h - c\dot{V}_{pzt}\left|h\right| \quad (27)$$

where*a*, *b* and *c* are the parameters of this model, *h*is the hysteresis variable. And the parameters identification is implemented by nonlinear least square toolboxrunning in Matlab environment.

The block diagram of the control with hysteresis compensation is shown in Fig. 22.The inverse B-W modelcan be cascaded to the physicalsystem as a feedforward hysteresis compensator. In order to improvestability of the tracking performance of the stage, a feedback controller is necessary. Therefore, a proportional-integral (PI) controller is employed to establisha feedforward-feedback hybrid controller. The schematic diagram of the hybrid controller is proposed in Fig. 23.

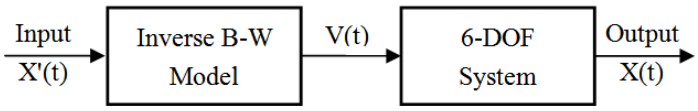

Figure 22 Block diagram of the 6-DOF system with hysteresis compensation

To test the tracking ability of the 6-DOF system under the control block diagram, six sinusoidal trajectory motion tests are conducted to evaluate the tracking performanceof the 6-DOF system.Fig. 24 shows the experimental results on the six sinusoidal trajectories. For three translational DOF trajectories, three sinusoidal trajectories with the same amplitude of 6μm and frequencies of 1 Hz were adopted

respectively. As shown in Fig. 24 (a-c), the maximum tracking errors can be reduced to ±0.1 μm, which with respect to the output displacement is as small as 1.67%.

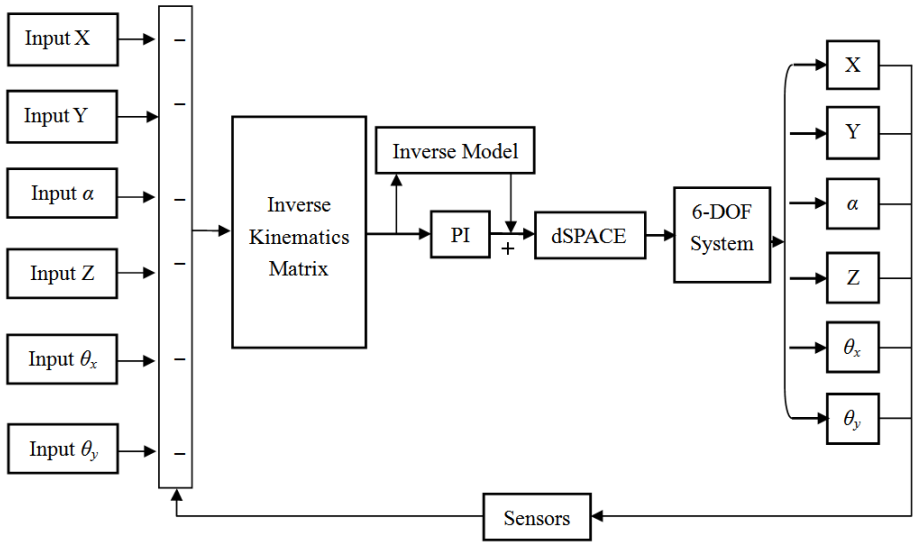

Figure 23 The schematic diagram of the hybrid controller

For three rotational DOF trajectories,Fig. 24 (d-f) shows three sinusoidal trajectories with the same frequencies of 1 Hz and amplitude of 180, 80, 80μrad, respectively. The maximumtracking errors ±5.01 μrad, +4.31 μrad and -4.56 μrad are observed in the motion, which with respect to the angular displacement is as large as 2.783%, 5.387% and 5.7%, respectively.

From the experimental results of uniaxial trajectoriestracking, the trackingaccuracy of translational DOF trajectories is higher than the rotational DOF trajectories. This result appears for several reasons, such as installation errors and measuring errors. However, the noise signal in experimental environment affects the measurement accuracy of the laser displacement sensors.

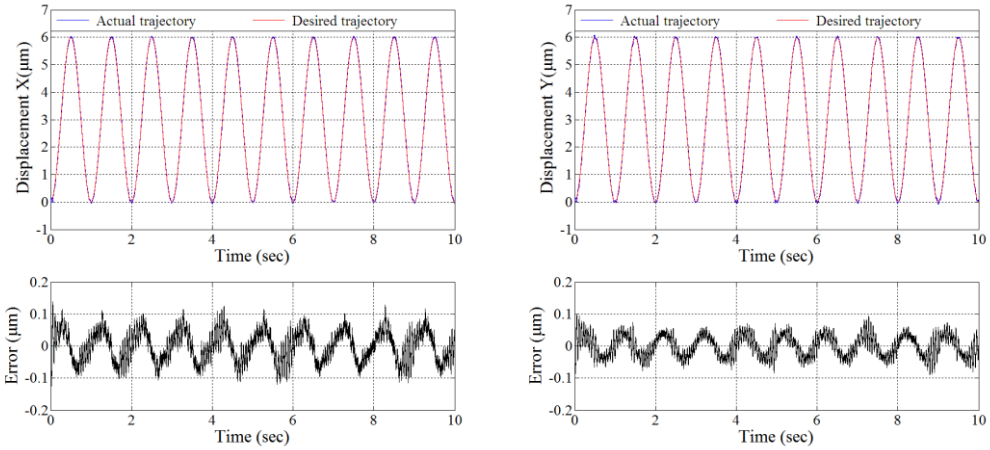

(a)

(b)

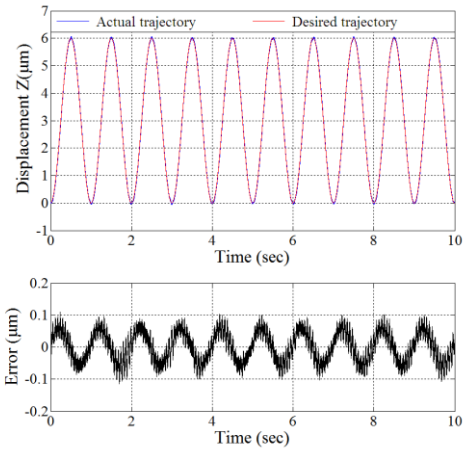

(c)

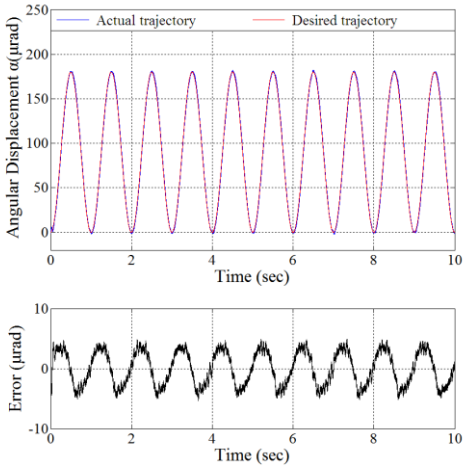

(d)

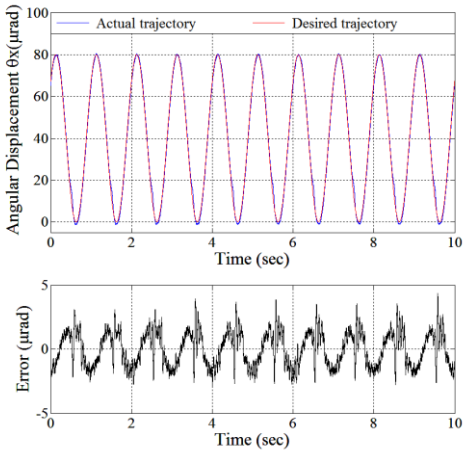

(e)

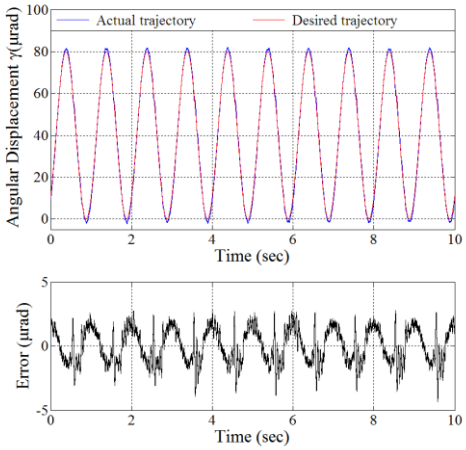

(f)

Figure 24 The result of 1 Hz sinusoidal motion tracking

In order to examine thetracking performances of the 6-DOF stage on multi-axis, experimental testing on the followingtrajectory are presented: (1) Two

samecirculartrajectories centered at point(3.0 μm, 3.0 μm) with a radius of 3.0 μm; (2) Two three-translational DOF trajectories are chosen as the reference trajectoriesdefined by equations (28) and (29), respectively.

$$\begin{cases} x(t) = 3 + 3\sin(2\pi t + 2\pi) \\ y(t) = 3 + 3\sin(2\pi t + 1.5\pi) \\ z(t) = 0.8t \end{cases} \tag{28}$$

$$\begin{cases} x(t) = 3 + 3\sin(2\pi t + 2\pi) \\ y(t) = 3 + 3\sin(2\pi t + 1.5\pi) \\ z(t) = 3 + 3\sin(2\pi t + 2\pi) \end{cases} \tag{29}$$

The experimental results are shown in Figs. 25 and 26. It provided the discrepancies between the desired and actual trajectory. The tracking errors in the X-, Y- and Z- axis are also recorded, respectively.

From the experimental result of bi-axial trajectoriestracking, as shown in Fig. 25(a), the maximum tracking error (-0.1985 μm in the *X*-axis and -0.1515 μmin the *Y*-axis) with respect to the output displacement is as large as 3.308%in the *X*-axis and 2.525%in the *Y*-axis, respectively. As shown in Fig. 25(b), the maximum tracking error (-0.1980 μm in the *Y*-axis and -0.1589 μmin the *Z*-axis) with respect to the output displacement is as large as 3.3%in the *Y*-axis and 2.648%in the *Z*-axis, respectively. For the three-translational DOF trajectories, as shown in Fig. 26(a) (the helical trajectory), the maximum tracking error (-0.2311 μm in the *X*-axis, -0.2097 μmin the *Y*-axis and -0.1015 μmin the*Z*- axis) with respect to the output displacement is as large as 3.852%in the *X*-axis, 3.495%in the *Y*-axis and 1.269%in the *Z*-axis, respectively. As shown in Fig. 26(b) (the circular trajectory), the maximum tracking error (-0.2835 μm in the *X*-axis, -0.2165 μmin the *Y*-axis and -0.1621 μmin the *Z*-axis)

with respect to the output displacement is as large as 4.725%in the *X*-axis, 3.608%in the *Y*-axis and 2.701%in the *Z*-axis, respectively.

Compared withthe uniaxialtrajectoriestracking, the multi-axis tracking performance of the 6-DOF system is slightly reduced. This is mainly due to the cross-axis couplings effects, installation errors, as well as the noise level of the displacement sensors and measurement circuits. Therefore, the future research work will be directed towards the laser interferometry based sensing and measurement and robust controller design to improve the tracking performance of the developed 6-DOF positioning system.

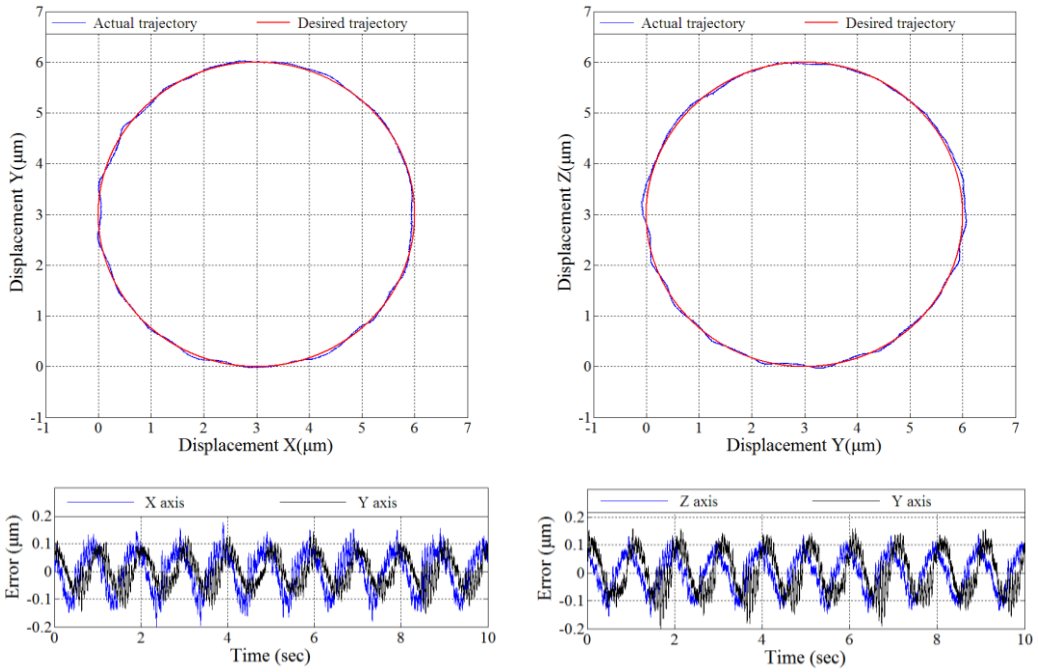

(a) (b)

Figure 25 The result of two-axis circular trajectory tracking: (a) X-, Y- axes and (b) Y-, Z- axes

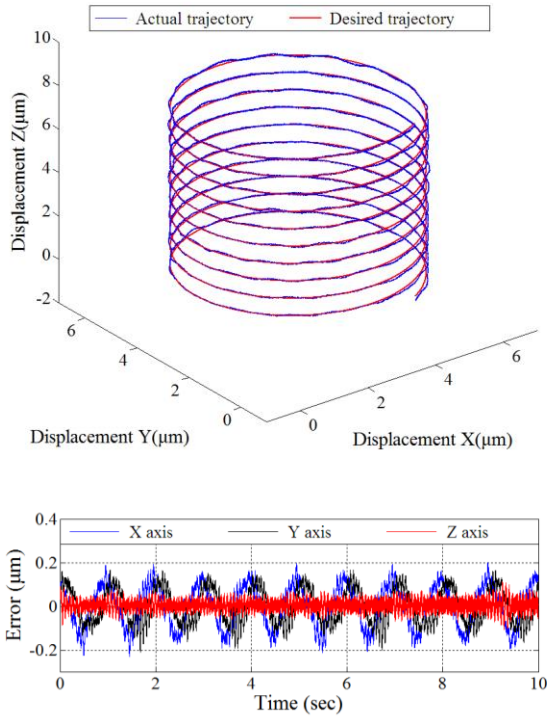

(a)

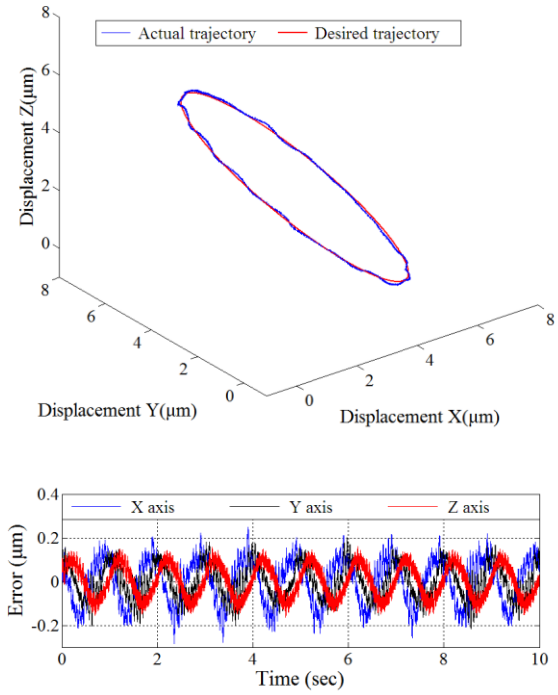

(b)

Figure 26 The result of three-axis translational trajectory tracking: (a) Helical trajectory and (b)

Circular trajectory

6 Conclusions

This paper presents a novel 6-DOF stage with thestudy on structural design, kinematics analysis, decoupling controller design, and experimental evaluation for the motion control of the stage.The 6-DOF positioning system are the integration oftwo differentkinds of 3-DOF positioning stages, an in-plane stage and an out-of-plane stage,both manufactured using the wire electrical discharge machining (WEDM) technology. The kinematic model of the 6-DOF system and the kinematictransformation matrix has been established. The static and dynamic characteristics of the stage have been investigated using FEA. In addition, the vibration testing experiment demonstrate that the design structure provides thehigh dynamic bandwidth with the lowest resonant frequency of 586.3 Hz.Experimental tests on the prototype stage with the decoupling control has beenconducted to verify theeffectiveness of decoupling control law. The proposed 6-DOF system has an effective workspace of 8.2 μm× 10.5 μm× 13.0 μm× 224 μrad × 105 μrad × 97 μrad. In order to improvecapability of the tracking performance of the stage, a feedforward-feedback hybrid controller has been established. The different motion trajectories have also been performed to present the good tracking performance of theproposed 6-DOF stage.

Acknowledgement

This research is supported by National Natural Science Foundation of China (Nos. 51175372, 51275337, 51205279, 51420105007), Reserved Academic Program of Peiyang Scholar,Program for New Century Excellent Talents in University (No. NCET-11-0374) and Tianjin Science and Technology Commission (No. 13JCQNJC04100)

References

[1] Wang F*, Li J, Liu S, Zhao X, Zhang D, Tian Y. An improved adaptive genetic algorithm for image segmentation and vision alignment used in microelectronic bonding. IEEE/ASME Transactions on Mechatronics 2014; 19(3):916-923.

[2] Wang F J*, Liang C M, Tian Y L, Zhao X Y, and Zhang D W. Design of a piezoelectric-actuated microgripper with a three-stage flexure-based amplification, IEEE/ASME Transactions on Mechatronics 2015; 20(5): 2205-2213.

[3] Liang C, Wang F*, Tian Y, Zhao X, Zhang H, Cui L, Zhang D, Ferreira P. A novel monolithic piezoelectric actuated flexure-mechanism based wire clamp for microelectronic device packaging. Review of Scientific Instruments 2015; 86(4): 045106.1-10.

[4] O. Payton, L. Picco, A. Champneys, et al.. Experimental observation of contact mode cantilever dynamics with nanosecond resolution. Review of Scientific Instruments 2011; 82(4): 043704-1-043704-5

[5] D. Wang, Q. Yang and H. Dong. A monolithic compliant piezoelectric- driven microgripper: design, modeling, and testing. IEEE/ASME Transactions on Mechatronics 2013; 18(1): 138-147

[6] M. Raghavendra, A. Kumar and B. Jagdish. Design and analysis of flexure-hinge parameter in microgripper. International Journal of Advanced Manufacturing Technology 2010; 49(9-12): 1185-1193

[7] M. Zubir, B. Shirinzadeh and Y. Tian. A new design of piezoelectric driven compliant-based microgripper for micromanipulation. Mechanism and Machine Theory 2009; 44(12): 2248-2264

[8] Wang F*, Zhao X, Zhang D, Ma Z, Jing X. Robust and precision control for a directly driven XY table. Proceedings of the Institution of Mechanical Engineers Part C-Journal of Mechanical Engineering 2011; 225(C5):1107-1120.

[9] Wang F, Ma Z, Gao W*, Zhao X, Tian Y, Zhang D. Dynamic modeling and control of a novel XY positioning stage for semiconductor packaging. Transactions of the Institute of Measurement and Control 2015; 37(2):177-189.

[10] Y. Tian, B. Shirinzadeh, D. Zhang. A flexure-based mechanism and control methodology for ultra-precisionturning operation. Precision Engineering 2009; 33(2):160-166.

[11] Y. Tian, B. Shirinzadeh, D. Zhang. Design and dynamics of a 3-DOF flexure-based parallel mechanism for micro/nano manipulation. Microelectronic Engineering 2010; 87(2):230-241.

[12] Y. Qin, B. Shirinzadeh, Y. Tian, D. Zhang and U. Bhagat. Design and Computational Optimization of a Decoupled 2-DOF Monolithic Mechanism. IEEE/ASME Transactions on Mechatronics 2014; 19(3):872-881.

[13] Y. Qin, B. Shirinzadeh, Y. Tian, D. Zhang. Design issues in a decoupled XY stage: Static and dynamics modeling, hysteresis compensation, and tracking control. Sensors and Actuators A: Physical 2013; 194:95-105.

[14] C. Li, G. Gu, M. Yang and L. Zhu. Design, analysis and testing of a parallel-kinematic high-bandwidth XY nanopositioningstage. Review of Scientific Instruments 2013; 84(12): 125111-1-125111-12.

[15] K. Cai, Y. Tian, F. Wang, D. Zhang, B. Shirinzadeh. Development of a piezo-driven 3-DOF stage with T-shape flexiblehinge mechanism. Robotics and Computer-Integrated Manufacturing 2016; 37(1): 125-138.

[16] D. Zhang, D.G. Chetwynd, X. Liu, Y. Tian. Investigation of a 3-DOF micro-positioning table for surface grinding. International Journal of Mechanical Sciences 2006; 48(12):1401-1408

[17] H. Kim, J. Kim, D. Ahn, D. Gweon. Development of a Nanoprecision 3-DOF Vertical Positioning System With a Flexure Hinge. IEEE Transactions on Nanotechnology 2013; 12(2): 234-245.

[18] H. Lee, H. Kim, H. Kim, D. Gweon. Optimal design and experiment of a three-axis out-of-plane nanopositioning stage using a new compact bridge-type displacement amplifier. Review of Scientific Instruments 2013; 84(11):115103-1-115103-10.

[19] B. Shao, L. Chen, W. Rong, C. Ru, M. Xu. Modeling and design of a novel precision tilt positioning mechanism forinter-satellite optical communication. Smart Materials and Structures 2009; 18(3):1-6.

[20] D. Kim, D. Kang, J. Shim, I. Song, D. Gweon. Optimal design of a flexure hinge-based XYZ atomic force microscopy scanner for minimizing Abbe errors. Review of Scientific Instruments 2005; 76(7): 073706-1-073706-6.

[21] Y. Yue, F.Gao, X. Zhao, Q. Ge. Relationship among input-force, payload, stiffness and displacement of a 3-DOF perpendicular parallel micro-manipulator. Mechanism and Machine Theory 2010; 45(5): 756-771.

[22] M Eichmann, T Krause, D Flühs, B Spaan. Development of a high-precision xyz-measuring tablefor the determination of the 3D dose rate distributions of brachytherapy sources. Physics in Medicine and Biology 2012; 57(22): N421-N429.

[23] M. Lu, S.Gao, Q. Jin, J. Cui, H. Du, H. Gao. An atomic force microscope head designed for nanometrology. Measurement Science and Technology 2007; 18(6): 1735-1739.

[24] P. Gao, S. Swei. A six-degree-of-freedom micro-manipulator based on piezoelectric translators. Nanotechnology 1999; 10(4): 447-452.

[25] R. Seugling, T. LeBrun, S. Smith, L. Howard. A six-degree-of-freedom precision motion stage. Review of Scientific Instruments 2002; 73(6): 2462-2468.

[26] Q. Liang, D. Zhang, Z. Chi, Q. Song, Y. Ge, Y. Ge. Six-DOF micro-manipulator based on compliant parallel mechanism with integrated force sensor. Robotics and Computer-Integrated Manufacturing 2011; 27(1): 124-134.

[27] R. Fung, W. Lin. System identification of a novel 6-DOF precision positioning table. Sensors and Actuators A: Physical 2009; 150(2): 286-295.

[28] D. Kang, D. Gweon. Development of flexure based 6-degrees of freedom parallel nano-positioning system with large displacement. Review of Scientific Instruments 2012; 83(3): 035003-1-035003-9.

[29] A.G. Dunning, N. Tolou, J. L. Herder. A compact low-stiffness six degrees of freedom

compliant precision stage. Precision Engineering 2013; 37(2): 380-388.

[30] Y. Ting, H.-C.Jar and C.-C. Li. Measurement and calibration for Stewart micromanipulation system. Precision Engineering 2007;31(3):226-233

[31] A. Boukari, J. Carmona, G. Moraru, F. Malburet, A. Chaaba, M. Douimi. Piezoactuators modeling for smart applications. Mechatronics 2011; 21(1): 339-349.

[32] L. Juhasz, J. Maas, B. Borovac. Parameter identification and hysteresis compensation of embedded piezoelectric stack actuators. Mechatronics 2011; 21(1): 329-338.

[33] C. Lin, P. Lin. Tracking control of a biaxial piezo-actuated positioning stage using generalized Duhem model. Computers and Mathematics with Applications 2012; 64(5): 766-787.

[34] M. Rakotondrabe. Bouc-Wen modeling and inverse multiplicative structure to compensate hysteresis nonlinearity in piezoelectric actuators. IEEE Transactions on Automation and Engineering 2011; 8(2): 428-431.

[35] Y. Liu, K. Chang and W. Li. Model reference adaptive control for a piezo-positioning system. Precision Engineering 2010; 34(1): 62-69.

[36] J. Park and W. Moon. Hysteresis compensation of piezoelectric actuators: The modified Rayleigh model. Ultrasonics 2010; 50(3): 335-339.

[37] X. Zhang and Y. Lin. Adaptive tracking control for a class of pure-feedback non-linear systems including actuator hysteresis and dynamic uncertainties. IET Control Theory and Applications 2011; 5(16): 1868-1880.

[38] T. Low and W. Guo. Modeling of a three-layer piezoelectric bimorph beam with hysteresis. J. MEMS1995; 4(4): 230-237.

[39] G. Gu, L. Zhu, C. Su and H. Ding. Motion control of piezoelectric positioning stages: modeling, controller design and experimental evaluation. IEEE/ASME Transactions on Mechatronics 2013; 18(5): 1459-1471.

[40] G. Gu, L. Zhu, C. Su, H. Ding and S. Fatikow. Modeling and control of piezo-actuated nanopositioning stages: A survey. IEEE Transactions on Automation Science and Engineering 2016; 13(1): 313-332.

[41] G. Y. Gu and L. M. Zhu. Motion control of piezoceramic actuatorswith creep, hysteresis and vibration compensation. Sensors and Actuators A: Physical 2013; 197:76-87.

[42] M. Rakotondrabe, C. Clevy, and P. Lutz. Robust feedforward-feedbackcontrol of a nonlinear and oscillating 2-DOF piezocantilever. IEEE Transactions on Automation Science and Engineering 2011; 8(3): 506-519.

[43] T. Tuma, A. Pantazi, J. Lygeros, and A. Sebastian. Nanopositioningwith impulsive state multiplication: A hybrid control approach. IEEE Transactions on Control Systems and Technology 2013; 21(4): 1352-1364.

[44] P.Ko,Y.WangandS.Tien. Inverse-feedforward and robust-feedbackcontrol for high-speed operation on piezo-stages.International Journal of Control 2013; 86,(2): 197-209.

[45] G. Gu, L. Zhu, C. Su, H. Ding and S. Fatikow. Proxy-based sliding mode tracking control of piezoelectric-actuated nanopositioning stages. IEEE/ASME Transactions on Mechatronics 2015; 20(4): 1956-1965.

[46] Y. Qin, B. Shirinzadeh, D. Zhang, Y. Tian. Compliance modeling and analysis of statically indeterminate symmetric flexure structures. Precision Engineering 2013; 37(2): 415-424.